

PHYSICO-CHEMICAL STUDIES OF THE OXIDATION OF
SOLID POTASSIUM IODIDE BY HALOGEN GASES

by

MAHENDRA DAS BAIJAL
B.Sc., Agra University, 1954
M.Sc., Agra University, 1956

A THESIS SUBMITTED IN PARTIAL FULFILMENT OF
THE REQUIREMENTS FOR THE DEGREE OF
DOCTOR OF PHILOSOPHY
in the Department of
CHEMISTRY

We accept this thesis as conforming to the
required standard

THE UNIVERSITY OF BRITISH COLUMBIA

May 1964

In presenting this thesis in partial fulfilment of the requirements for an advanced degree at the University of British Columbia, I agree that the Library shall make it freely available for reference and study. I further agree that permission for extensive copying of this thesis for scholarly purposes may be granted by the Head of my Department or by his representatives. It is understood that copying or publication of this thesis for financial gain shall not be allowed without my written permission.

Department of Chemistry

The University of British Columbia,
Vancouver 8, Canada

Date June 19, 1964

ABSTRACT

The mechanism of oxidation of Potassium iodide by Chlorine and Fluorine gas has been studied using powdered KI, pressed pellets and single crystals (pressed pellets only in the case of Fluorine). The electrical conductivity of a KI pellet has also been determined as a function of temperature. The major part of the experimental work concerns changes in D.C. electrical conductivity during reaction.

The main conclusions are as follows:

- (a) The room temperature conductivity of KI is always higher than that obtained by extrapolating the impurity-range, and the activation energy below about 92° C. is very small; this is tentatively attributed to a space-charge effect.
- (b) In the KI/Cl₂ reaction, the products are invariably KCl and I₂ in various forms (including V-Centres), although polyhalides are thermodynamically more stable. Thus the reduction of Chlorine occurs in a manner which does not allow reorganization to ICl₂⁻.
- (c) In pressed pellets, the conductivity always increases at the start of oxidation, but the enhanced conductivity may be ionic or electronic in different circumstances, and the initial increase may be followed by several alternative

processes which are structure-sensitive. There is an inverse correlation between initial conductance and reactivity which is interpreted in terms of competition between (i) trapping of positive holes at isolated cation vacancies and (ii) nucleation of solid Iodine at grain boundaries.

(d) Unpressed powders show no increase in conductance during reaction; this is attributed to preferential oxidation of bound surface states.

TABLE OF CONTENTS

	<u>Page</u>
Title Page	i
Abstract	ii
Table of Contents	iv
List of Figures	viii
List of Tables	xi
Acknowledgements	xiii
INTRODUCTION	
A. Known Reactions of Ionic Solids	1
B. Imperfections in Alkali Halides	3
(i) Ionic Point Defects	4
(ii) Electronic Defects	11
(iii) Dislocations	3
(iv) Evidence for the Trapping of Holes	
Singly and in Pairs	16
C. Previous Work on Alkali Halide/Halogen Systems	17
(i) Study of the KBr/Cl ₂ System by Kinetic, Microscopic, and Gravimetric Techniques	17
(ii) Optical Evidence for the Production of V-Centres by Chemical Means	18

(iii) Electronic Defects as Reaction Intermediates in Na ³⁶ Cl/H ₂ O-System	21
D. Objects of the Present Work	23
EXPERIMENTAL	
A. Preparation of KI Samples	25
(i) Large Particles	25
(ii) Small Particles	25
(iii) Small Particles to which Iodine Was Added	25
B. Determination of the Surface Area of Small Particles	27
(i) Apparatus	27
(ii) Calculation of Surface Area	27
C. Halogen Handling System	28
(i) Chlorine Purification System	29
(ii) Fluorine Handling System	32
D. Measurement of D.C. Electrical Conductivity	32
(i) Conductivity Cells	32
(ii) Electronic Equipment and Circuits	34
(iii) Procedure (including Polarization Effects)	40
(iv) Determination of Conductivity as a Function of Temperature	42

Page

E. Analysis of Reaction Products	44
(i) Characterization of Reaction Products by X-Ray Diffraction	44
(ii) Determination of Iodine by Volumetric Analysis	45
(iii) Determination of Halide Ions by Potentiometric Titration	45
RESULTS	
A. Study of the Reaction Products and Kinetics (KI/Cl ₂ System)	46
(i) X-Ray Diffraction (Powdered Samples)	46
(ii) Kinetics (Powdered Samples)	46
(iii) Potentiometric Determination of Halide Ions (Pressed Pellets)	47
B. The Electrical Conductivity of Pure KI	50
(i) Room Temperature Conductivity	50
(ii) Conductivity as a Function of Temperature	52
C. Changes of Electrical Conductivity during Reaction of KI Samples (Pressed Pellets) with Cl ₂ (g) or F ₂ (g)	57
(i) Types of Reaction	57
(ii) Type A Reactions	57
(iii) The Initial Rise in Conductivity	61
(iv) Type B Reactions	65

(v) The Appearance of the Reacted Pellets	70
D. Changes of Electrical Conductivity during the Reaction of Other Types of KI Sample with $\text{Cl}_2(\text{g})$	70
(i) Single Crystal	70
(ii) Powder	71
DISCUSSION	
A. Ionic Conductivity of KI as a Function of Temperature	73
B. The Nature of the Products	77
C. Reaction Steps in the Surface	78
D. Reaction Steps in the Bulk	80
E. Type A Behaviour	84
(i) Type A_1 Decay	86
(ii) Type A_2 Decay	87
F. Type B Behaviour	88
G. Factors Determining the Type of Reaction	91
H. Oxidation of Unpressed Powders	92
APPENDIX	
Summary of Experimental Results	94
Tables VI - XV	94-103
Figure 26	104
BIBLIOGRAPHY	105-108

LIST OF FIGURES

	<u>Page</u>
INTRODUCTION	
Figure 1. Ionic Defects in Alkali Halides	10
Figure 2. Models of V-Centres	14
Figure 3. Photo Micrograph of a Reacted Potassium Bromide Crystal Showing Bromine-Filled Cavities	19
Figure 4. Chemically Produced V-Bands in Alkali Halides	22
EXPERIMENTAL	
Figure 5. Vacuum Filtration Apparatus	26
Figure 6. Chlorine Purification System	31
Figure 7. Conductivity Cell X	33
Figure 8. Conductivity Cell Y	35
Figure 9. Guard Ring Arrangement	36
Figure 10. Circuit Diagram for the Procedure	38
Figure 11. Circuit Diagram for the Switch Gear	39
RESULTS	
Figure 12. Reaction of Powdered KI with Cl ₂ ; Zero-order Plot	48
Figure 13. Potentiometric Titration Curves	49
Figure 14. Electrical Conductivity of KI, 250° C. to 680° C. (Lehfeldt)	53

- Figure 15. Electrical Conductivity of KI, 22° C. to 330° C. (This Work) 54
- Figure 16. Reaction of Pressed Pellets with Cl₂; Conductivity and Polarization in Type A and Type B Behaviour 58
- Figure 17. Plots to Test Shape of Conductivity-Time Curves: Type A₁, First-Order Decay; Type A₂, Second-Order Decay; Type B, Parabolic Rise in Conductivity 60
- Figure 18. First-Order Plot, Type A₁ Reaction 63
- Figure 19. Correlation of Rate Constant for Initial Rise with Initial Conductivity of Pellet 66
- Figure 20. Reaction of Pressed Pellet with F₂; Conductivity and Polarization Curves 68
- Figure 21. Type B, Parabolic Rise in Conductivity (KI/F₂ System) 69
- Figure 22. Reaction of Single Crystal with Cl₂; Comparison of Conductivity Changes and Kinetics of Iodine Formation 72
- Figure 23. Fit of Cl₂ Molecule and Misfit of ICl₂⁻ in an Anion Vacancy in KI 79
- Figure 24. Proposed Mechanism of a Type A Reaction 82

Page

Figure 25. Proposed Mechanism of a Type B Reaction

83

APPENDIX

Figure 26. Summary of KI/F₂ Runs

104

LIST OF TABLES

	<u>Page</u>
EXPERIMENTAL	
Table 1. Extract from the Laboratory Diary	43
RESULTS	
Table 2. Initial Conductivity of Various Samples of KI at 23° C.	51
Table 3. Activation Energies of the Electrical Conductivity of KI	55
Table 4. Correlation of Particle Type with Temperature of First Break in Log C vs. 1/T Curve	56
Table 5. Behaviour after Initial Rise in Conductance	59
APPENDIX	
Table 6. Kinetic Results for the KI/Cl ₂ Reaction	94
Table 7. Tabulated Data from Electrical Conductivity Measurement in KI/Cl ₂ Reaction	95-96
Table 8. Electrical Conductivity of KI, 250° C. to 680° C. (Lehfeldt)	97
Table 9. Electrical Conductivity of KI, 22° C. to 330° C. (This Work)	97
Table 10. Specification from Mallinckrodt Chemical Works of the KI Used in This Work	98

Table 11. Data from KI/F ₂ Reactions	99
Table 12. Polarization Behaviour in the Course of KI/Cl ₂ and KI/F ₂ Reactions	100
Table 13. Initial Rise in Conductance	101
Table 14. Type B Behaviour in an I ₂ Added Pellet	102
Table 15. Height of the Fermi Level above Cation Vacancy Level at the End of Oxidation, from C _∞ /C ₀	103

ACKNOWLEDGEMENTS

I am deeply indebted to Dr. L. G. Harrison for guidance throughout the present work.

I am grateful to Professor C. A. McDowell for providing departmental facilities.

My thanks are due to Dr. N. Bartlett for a discussion on polyhalides and for supplying Fluorine gas, to Dr. R. J. Adams for making the surface area measurement apparatus available, and to Mr. R. C. Catton for assistance in the preparation of diagrams.

INTRODUCTION

A. Known Reactions of Ionic Solids

As a general class of reactions of solids, oxidation and reduction of ionic crystals has received so little attention that it is not even listed in most classifications.

Studies of reactions involving an ionic solid as one reactant have been principally of two kinds (1,2), reduction of cations (the photographic process) and thermal decomposition. In the reduction of cations in silver halides, the most important feature of the process seems to be the role of the surface, which is the reaction zone in the small particles of photographic emulsions, and the role of dislocations and grain boundaries in large crystals (1).

While in thermal decomposition the primary step possibly occurs at the surface of the ionic solid, the new solid phase may form in the bulk of the solid or at the surface. In this type of reaction nucleation processes are of great importance (2).

By contrast, reactions involving the oxidation of anions by external oxidizing agent have been almost completely neglected. Yet such processes may be expected, a priori, to be particularly suitable for studying the relationship between conductivity and reactivity, which was one of the original

objectives of Wagner's work (3) on solid state reactions some thirty years ago.

Such reactions in alkali halides have the interesting feature that the path for electronic conduction must be provided by the reaction itself, probably by the production of positive holes in the anion band.

It is thus to be expected that trapped-hole centres may be important intermediates in the reaction mechanisms (or even final products of the reactions). There is still much that is not known about both the structure of trapped-hole defects and their possible roles as intermediates in reactions of ionic solids. Although a few structures are definitely known (V_k centre, H-centre, " F_3^{2-} ion"), the centres responsible for the principal optical absorptions of X-irradiated and halogen-doped alkali halides in the u.v. region (V_1 , V_2 , V_3 and V_4 bands) are still uncertain. Colour centres have been discussed by Billington and Crawford (4) in connection with the mechanism of radiation damage in alkali halides, and some useful kinetic evidence on the colouration and bleaching of trapped-electron centres (F, R, M, N etc.) has been obtained (5,6), but kinetic evidence on the V centres is still lacking.

The present work constitutes the first reported

kinetic study of the KI/Cl_2 and KI/F_2 reactions. Concurrently, the system KBr/Cl_2 has been studied from the kinetic viewpoint by Morrison and Nakayama (7), using an entirely different experimental approach.

Simultaneously with the work reported in this thesis, other workers in this laboratory have been studying the systems KI/Cl_2 , KBr/Cl_2 , NaCl/F_2 and $\text{Na}^{36}\text{Cl}/\text{Cl}_2$ by various experimental methods, including visible-u.v. spectrophotometry, radioactive tracer studies (^{36}Cl) and microscopical examination. This work is reported in part C of this introduction. The microscopical work on KBr/Cl_2 is particularly relevant to the mechanisms proposed in this thesis for the KI/Cl_2 reaction.

B. Imperfections in the Alkali Halides

Defects in alkali halides are of three types:

- (i) Ionic Point Defects: These are discussed in more detail below.
- (ii) Electronic Defects: These are of great importance in my reaction mechanisms, and are discussed below.
- (iii) Dislocations: The detailed structure of these has not been important in the present work, and will not be discussed. They may be important in my reaction mechanisms in controlling vacancy concentrations, and providing paths for

low temperature ionic migration.

(i) Ionic Point Defects:

Of these the most important is the vacant lattice site (anion or cation) (see Figure I(a)). These can exist subject to two conditions:

(a) In thermal equilibrium, in the bulk of the crystal, the product of cation and anion vacancy concentrations is a constant dependent only on temperature. The mole fractions of cation vacancies X_1 and anion vacancies X_2 are related by the expression

$$X_1 X_2 = X_0^2 = \exp(-g/KT) \quad (1)$$

where X_0 is the equilibrium mole fraction of vacancies (cation or anion) in the pure crystal, g is the change in the Gibb's free energy on taking a normal lattice ion-pair to the surface of the crystal, apart from the configurational entropy contribution, and KT has its usual meaning. X_1 is equal to N_1/N , where N_1 is the number of cation vacancies and N the total number of sites in the cation sub-lattice. Because X_1 is frequently much less than unity, N may usually be set equal to the number of cations in the crystal (8).

(b) The crystal as a whole must be electrically neutral, although there can be a charge separation between the bulk, on the one hand, and external surfaces, and dislocations

on the other.

Vacancies can arise in several ways:

(a) They may be formed by the motion of an anion into an interstitial position (Frenkel Defects (9); common in silver halides (10); but not alkali halides (11)).

(b) Vacancies may be formed at the surface, resulting in expansion of the lattice by a number of sites equal to the number of vacancies (Schottky Defects (12), (13), (14)).

Calculations of the energy of formation of Frenkel and Schottky defects indicate that the latter type is favoured if there is an approximate equality in size of the cations and anions, if the dielectric constant is low, and if the Van der Waals contribution to the lattice energy is low. The alkali halide crystals are of this type. The opposite conditions exist in silver halides and so Frenkel defects are favoured.

Calculations of W_s (where W_s represents the energy required to form a Schottky defect), and W_i (where W_i represents the energy required to form a Frenkel defect) have been made by Jost (15), Schottky (13), and Mott and Littleton (16). However, calculations of W_s have been made more accurately by Dreyfus and Nowick (17), and Fumi and Tosi (18). Mott and Littleton find a value of $W_i = 2.9$ eV. for Na^+ in NaCl, while the value they compute for W_s is 1.9-2.0 eV. for NaCl, KCl

and KBr. Dreyfus and Nowick's values of W_s for NaCl and KCl are 2.1 ± 0.06 eV. and 2.22 ± 0.12 eV. The latter values agree with Fumi and Tosi's values (18).

These theoretical results indicate, then, that Schottky defects are predominant in alkali halides.

(c) Vacancies may arise as a result of the presence of multivalent impurities, to maintain electrical neutrality of whole lattice (see Figure I(b)).

Pick and Weber (19) have studied the density of KCl-CaCl₂ solid solutions, and find that the densities vary with composition in the way one would expect if the substitution of a Ca⁺²-ion for a K⁺-ion resulted in the formation of a K⁺-ion vacancy. Unlike the thermally-created defects, the concentration of impurity induced vacancies is independent of temperature, being determined solely by the concentration of multivalent impurities. If C denotes the mole fraction of divalent impurity cations added to a 1:1 crystal and if every added impurity ion is compensated for by the formation of a cation vacancy, then electroneutrality requires

$$X_1 = C + X_2 \quad (2)$$

(where X_1 and X_2 have their usual significance). Two extreme cases may be distinguished; at high temperature in a pure

crystal,

$C \ll X_0$ (where X_0 has its usual meaning) and therefore

$X_1 = X_2 = X_0$ (Intrinsic Region).

While at low temperature,

$C \gg X_0$, and so

$X_1 = C$ (Structure Sensitive Region or
Impurity Region) (8)

Combination of Charged Defects (see Figure I(c))

Since vacancies carry an effective charge, they may combine with each other or with multivalent impurities, by electrostatic interaction. Important structures of this type are:

(a) Vacancy-pair

A vacancy-pair is formed as a result of the combination of a cation vacancy with an anion vacancy. The vacancy-pairs are electrically neutral entities, and do not contribute to the electrical conductivity, but they can move through the crystal and thus contribute to diffusion processes. The binding energy of a vacancy-pair is reasonably large, of the order of $W_s/2$ (where W_s is the energy required to form a Schottky defect), and a substantial concentration of such pairs is to be expected (20,21). Most of the experimental attempts (22,23,24) to demonstrate the existence of vacancy-

pairs in the alkali halides have been unsuccessful, but, in principle, one must take account of their possible existence (20,21,25).

It has been suggested that the possible existence of vacancy-pairs is important to colour centre problems, since the creation and transformation of these centres at low temperatures is most easily explained in terms of the motion of these defects.

Theoretical estimates of the activation energy of mobility of vacancy-pairs have been somewhat equivocal about this possibility. The first estimate by Dienes (26) gave a low activation energy and supported the concept of low temperature mobility; but Tharmalingam and Lidiard (27) recently published a much higher estimate of the activation energy.

(b) Vacancy-impurity Complex

The impurity-generated defect tends to be associated into a "complex" comprising the impurity ion and the defect on adjacent sites. Increase in temperature tends to dissociate the complexes, giving rise to free vacancies. Experimental and theoretical evidence has been obtained that such "complexes" do, indeed, exist in many impurity-doped crystals.

Dreyfus and Nowick's (28) results on the D.C. Ionic

Conductivity of NaCl Crystals doped with various divalent impurities can be completely explained right from above 400° C. (below the intrinsic region) down to -35° C. in terms of the concentration of the multivalent cationic impurities present in the lattice, their association with the cation vacancies, and the precipitation of impurity ions.

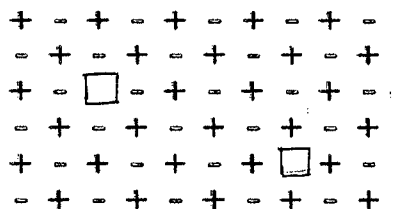
Interaction of Vacancies with Surfaces and Dislocations

(a) Space-charge Effect (see Figure I(d))

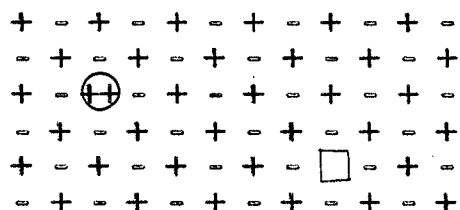
It has been shown theoretically (29,30) that external surfaces will acquire an excess of anion vacancies balanced by a space-charge of cation vacancies, if the energy of formation of an anion vacancy exceeds that for a cation vacancy. Lehovc (29) represents the effect of space-charge on conductivity by a width B which must be added to the true width of the crystal to give its extra conductivity. This extra conductivity is proportional to the surface area, and the extent of the space-charge is strongly temperature-dependent, and becomes larger than 1μ , (i.e. larger than the probable spacing between dislocations in many crystals) at any temperature below about 300° C. At $T > 600^\circ \text{K}$, $B \leq 1\mu$ for NaCl, but at room temperature Lehovc's equation gives B as about 1 cm. Thus the cation vacancy concentration may be completely controlled by dislocations. The theory

FIGURE 1

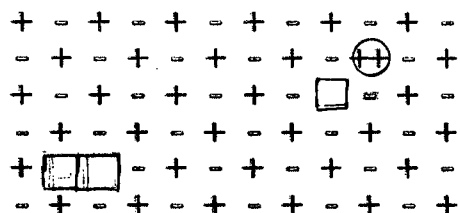
IONIC DEFECTS IN THE ALKALI HALIDES (TWO-DIMENSIONAL MODEL)



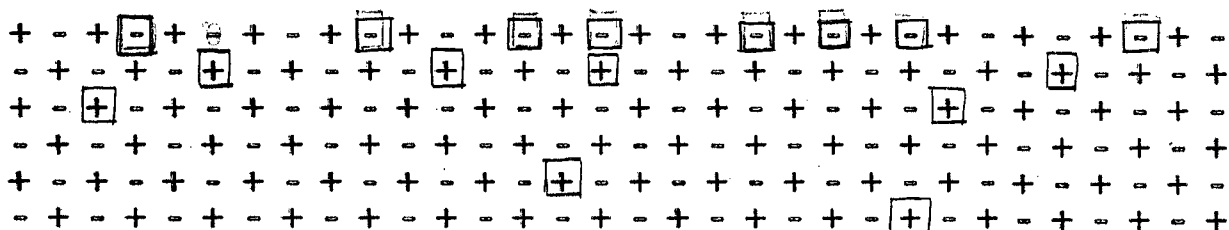
(a) Thermally created Schottky defect (cation and anion vacancy)



(b) Cation vacancy produced by divalent impurities



(c) Association effects. Impurity-vacancy complex & vacancy pair



(d) Space-charge effect near to the surface

of the space-charge needs to be amended for the case in which the finite size of the crystal is important.

(b) Charged Dislocations

The difference in the energy of formation of positive and negative ion vacancies in an ionic crystal also causes the dislocations to be charged (30) when the system is in thermal equilibrium. The charged dislocations are surrounded by a sheath of vacancies of predominantly the opposite sign. A grain boundary (or mosaic boundary) should also be charged and surrounded by a balancing layer of charge. The presence of divalent impurities modifies the magnitude of the charge, and may even reverse it. At low temperatures these (divalent) impurities cause the sign of the charge on a dislocation to reverse. (The interpretation of the first-order decay of conductance below room temperature of quenched samples of NaCl as observed by Dreyfus and Nowick (28), should presumably be in terms of the combination of vacancies with charged dislocations.)

(ii) Electronic Defects

These defects may be obtained in alkali halide crystals as a result of the following changes:

(a) by the introduction of electrons into the conduction band and subsequent trapping (trapped-electron centres);

(b) by the removal of electrons from the valence band and trapping of the resulting positive holes (trapped-hole centres).

Trapped-electron centres (or Electron-excess Centres) and trapped-hole centres (or Electron-deficit Centres) are collectively known as Colour Centres.

In chemical terms, trapped-electron centres increase the power of a substance to act as a reducing agent. They may often be thought of as arising from ionization of dissolved alkali metal atoms and may be formed by the dissolution of alkali metal atoms in the host lattice. Similarly, trapped-hole centres may be regarded as dissolved halogen atoms or molecules. They decrease the power of a substance to act as a reducing agent. They have been formed in alkali bromides and iodides by the dissolution of halogen atoms or molecules in the host lattice.

Centres of both types can be formed simultaneously by X-irradiation of alkali halides, which involves direct excitation of electrons from the valence band to conduction band and may be followed by trapping of both electrons and holes.

Structures of Colour Centres

(a) Trapped-electron Centres

The best known example of a trapped-electron centre is the F-Centre, wherein an electron is trapped in an anion

vacancy. Other centres of this kind are F' and aggregate centres, which all contain more than one trapped electron. Trapped-electron centres are detected by their absorption in the visible region of the spectrum. They will not be discussed further, as they have not been important in the present work.

(b) Trapped-hole Centres

The structures of trapped-hole centres have been the cause of much speculation. Thus models of these centres have been proposed by Seitz (20,21), Nagamiya (31), Burstein and Oberly (32), Varley (33), and St. James (34). The models proposed by Seitz (20,21) (see Figure 2), based upon a supposed analogy with the trapped-electron centres, have stimulated the most research. For the centres which are stable at room temperature, Seitz proposed that the trapping site is a pair of cation vacancies, and that the V_3 -Centre contains a single positive hole, while the V_2 -Centre has two. Seitz's approach to V-Centres failed to take note of the strong tendency of halogen atoms to form covalent bonds, and it now seems clear that, in general, the V-Centres are stabilized more by covalent bonding than by electrostatic interaction with vacancies.

Harrison (35) has suggested a chemical notation (see Figure 2) for V-Centres. In this notation, a and c

FIGURE 2
MODELS OF V-CENTRES

Defect	Seitz's Models	Harrison's Notation
F		(a)
(V ₁)		$\text{Cl}(\text{a})^+(\text{c})^-$
(V ₂)		$\text{Cl}(\text{a})_2^{++}(\text{c}_2)^{-}$
(H)		$\text{Cl}(\text{a})^+(\text{ac})$
(V ₃)		$\text{Cl}(\text{a})^+(\text{c}_2)^{-}$
(V ₄)		$\text{Cl}(\text{a})^+(\text{ac}_2)^{-}$

represent anion and cation sites, and ion signs for structures within the solid represent effective charges. Thus a^+ and c^- are vacant sites, $I(a)^+$ is a positive hole, and $I(a)_2^{2+}(c_2)^{2-}$ is a pair of holes trapped by two cation vacancies. This notation is useful in writing chemical equations involving V-Centres as reagents or products.

The only trapped-hole centres for which the structures are definitely known are:

- (1) the V_k -Centre which consists of an X_2^- (X = halogen) molecule-ion in a normally perfect lattice where it occupies 2 anion vacancies ($X(a)_2^+$ in Harrison's notation);
- (2) the H-Centre which consists of a X_2^- molecule-ion situated at a single halide ion site along with 2 halide ions adjacent to this site, and thus involves 4 halogen nuclei distributed over three anion sites ($X_2(a)$ or $X_4(a)_3$ in Harrison's notation);
- (3) the " F_3^{2-} ion" which resembles Seitz's model of V_4 -Centre, and consists of a positive hole localized over three fluoride ions ($F(a)_3^+(ac_2)^-$ in Harrison's notation).

These centres do not correspond to any of the strong optical absorption bands numbered V_1 - V_4 in the various alkali halides, and the structures giving rise to these bands are still uncertain.

At present the various structures due to different

V-bands are very uncertain and extensive further studies are needed. However, it seems quite likely that some of the centres corresponding to the known V-bands represent holes trapped in pairs, which will give no E.S.R. signal and for which the optical spectra have not proved very informative. For these centres, indirect evidence from kinetic studies is likely to remain important.

(iv) Evidence for the Trapping of Holes Singly and in Pairs

Some direct evidence by paramagnetic resonance and other studies has been obtained on the centres containing a single trapped hole.

(1) The identification of the F_3^{2-} (or $F(a)_3^+(ac_2)^-$) radical ion by Cohen et al. (36) in X-rayed LiF at 20° K. has shown the hole to be localized over three fluoride ions.

(2) Känzig (37) has found other trapped-hole centres in LiF X-rayed at 77° K. Due to their stability it has been suggested that the hole in these centres is associated with cation vacancy.

(3) Luckey (38,39) has measured the electrical conductivity of halogenated Ag-halides, and has found evidence for the trapping of holes singly (the concentration of positive holes is proportional to the square root of the pressure of halogen introduced).

The evidence on the trapping of holes in pairs has been

rather indirect.

(1) Mollwo (40) in his early work on additively coloured KBr and KI found the concentration of the colour centres varying directly as the first power of the pressure of the diatomic gas.

(2) The best known V-bands in KI and KBr resemble the spectra of linear tri-halide ions in solution (41,42). A tri-halide ion would represent the result of the interaction between a halogen molecule (2 positive holes) and a surrounding halide ion.

C. Previous Work on Alkali Halide/Halogen Systems

(i) Study of the KBr/Cl₂ System by Kinetic, Microscopic, and Gravimetric Techniques

Morrison and Nakayama (43) have studied recently the reaction of single crystals of Potassium bromide with Chlorine gas using kinetic, microscopic, and gravimetric techniques. Their main conclusions are:

(1) At room temperature, the kinetics of the reaction indicates that the initial step in the reaction is a nucleation process.

(2) From microscopic and other experimental measurements, the conclusion reached is that the reaction is initiated at

points on the crystal surface where local strain has been created by, e.g., mechanical damage or precipitation of impurities. No correlation has been found between nucleation sites and the points where dislocations or low-angle grain boundaries emerge at the local surface.

Morrison and Nakayama did not, however, examine the reacted samples for the location of the halogen products, and they did not look for V-Centres. Catton (44), studying the same reaction (KBr/Cl_2), in a microscopical examination of the reacted sample (KBr) has discovered bromine-filled cavities about 30μ beneath the surface of the crystal (see Figure 3). (The mechanism proposed for KI/Cl_2 reaction in this thesis preceded the direct observation of halogen-filled cavities by Catton.)

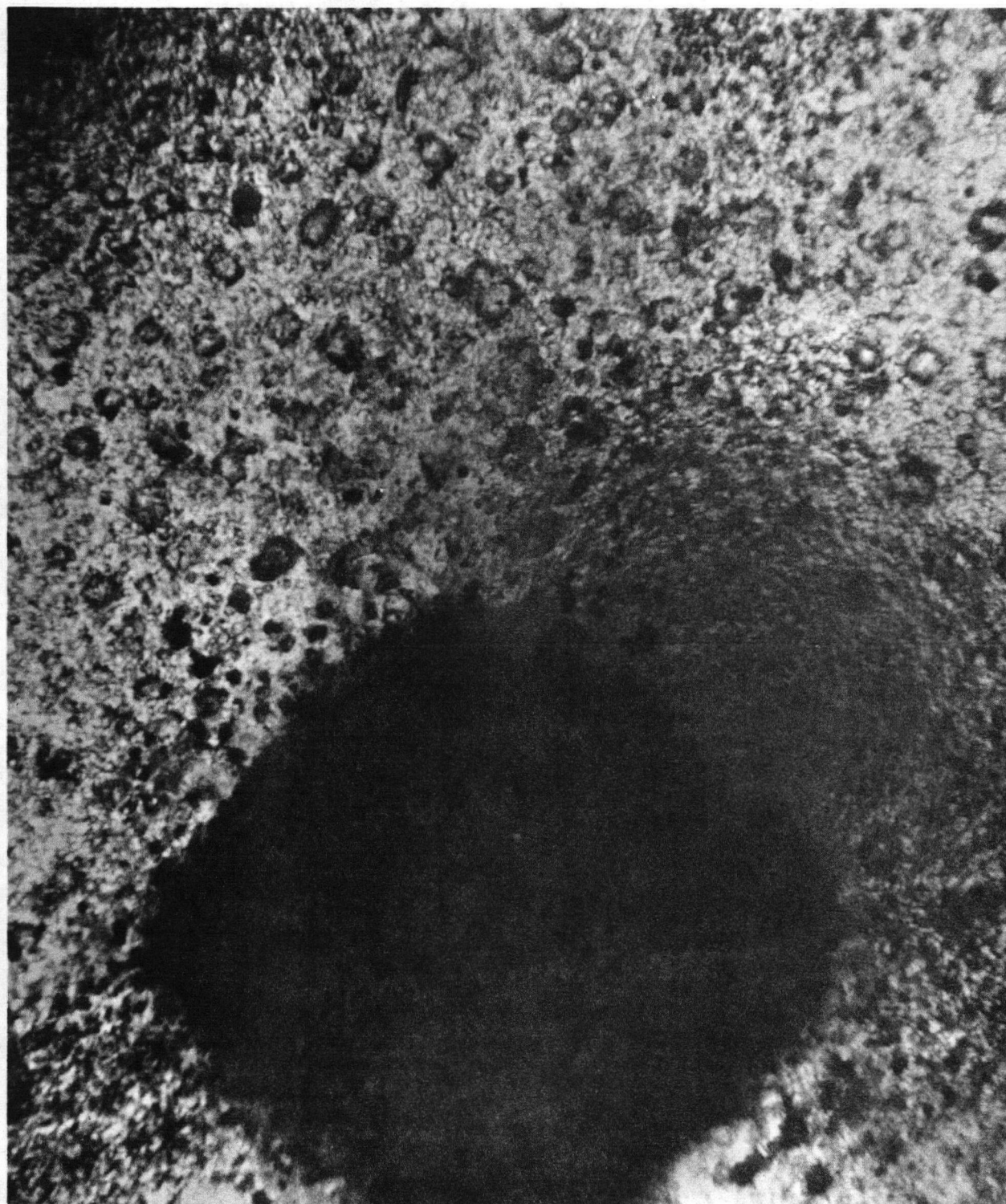
(ii) Optical Evidence for the Production of V-Centres by Chemical Means

(a) KI/Cl_2 System

Spectroscopic work by Bird (45) on this system, using Harshaw single crystals of KI was done simultaneously with the present work. Bird found V-Centres as the principal products of the reaction. He obtained absorption peaks at 2800 \AA and 3600 \AA (see Figure 4(a)), corresponding to the best known V-bands of KI. Uchida et al. (46) found evidence

FIGURE 3

PHOTO MICROGRAPH OF A REACTED POTASSIUM BROMIDE CRYSTAL
SHOWING BROMINE-FILLED CAVITIES



that in KI both 2800 Å and 3600 Å absorption bands arise from the single centre, but Bird found evidence that these two absorption bands arise from two different centres. He found that the ratio of these two peaks' heights was not always the same when these peaks were produced by room temperature oxidation of KI. Nakai (47) in his work on KBr has also found that the two principal absorption bands do not arise from the same centre. For KI it has been suggested (41,42) that the double-peaked spectrum resembles the solution spectrum of I_3^- , suggesting that the trapped-hole centre is a similar linear tri-halide ion. However, if the two peaks are confirmed to be independently variable, this analogy is incorrect. It would still be quite possible, however, that one of the absorptions represents an I_3^- ion or some other form of molecular iodine.

(b) KBr/Cl₂ System

Catton (44) in a recent study of the oxidation of Harshaw single crystals of KBr by Chlorine gas at room temperature has found an absorption band in the system at 2700 Å (see Figure 4(b)) - corresponding to one of the bands observed by Mollwo.

(c) NaCl/F₂ System

Harrison et al. (48) have studied the oxidation of

single crystals of NaCl by Fluorine gas at room temperatures (see Figure 4(c)). Their results are as follows:

(1) For polished crystals, V-Centres were the principal products, although the extent of the overall reaction was rather small. The V-Centres formed absorbed at $2150 \overset{\circ}{\text{A}}$, suggesting that they were V_3 -Centres (Seitz's model). Another absorption band at $3400 \overset{\circ}{\text{A}}$ was accounted for by the presence of Chlorine gas.

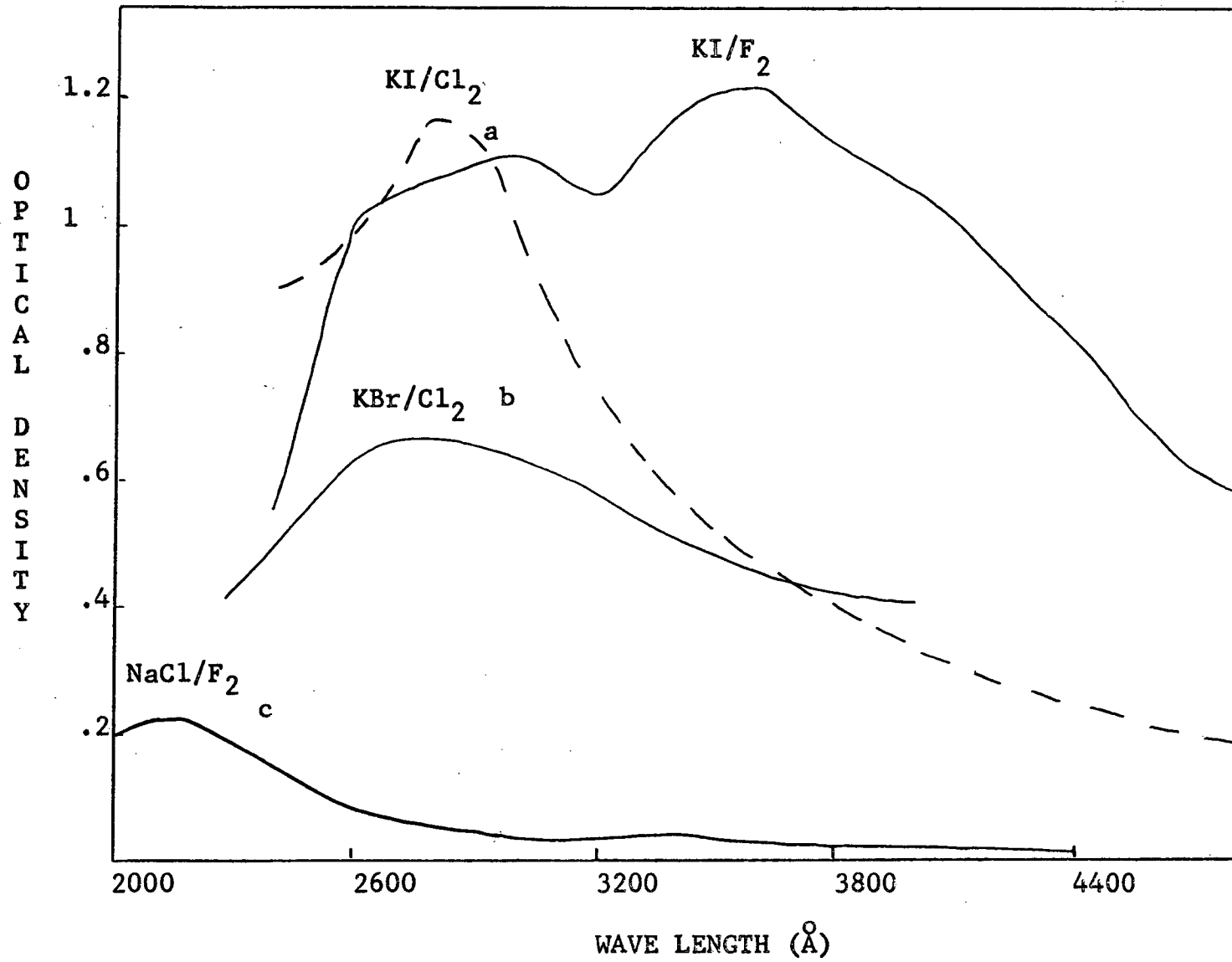
(2) For scratched and quenched crystals, an extensive reaction took place with the formation of a crystalline phase (probably NaF) on the surface and Chlorine inside the crystal. A small V-band was obtained which was shifted towards $2300 \overset{\circ}{\text{A}}$ and is presumably a V_2 -Centre.

To account for the extensive reaction observed in this case, they suggest that sites are available on the surface to facilitate the nucleation of the new alkali halide lattice while the nuclei of halogen probably appear below the surface of the crystal. (As in the case of KBr/ Cl_2 ; no microscopical observations have yet been made.)

(iii) Electronic Defects as Reaction Intermediates in $\text{Na}^{36}\text{Cl}/\text{Cl}_2$ System

Adams (49) has studied the exchange of ^{36}Cl , originally incorporated in the NaCl (solid) with gaseous Chlorine,

FIGURE 4 - CHEMICALLY PRODUCED V-BANDS IN ALKALI HALIDES



and has found that the extent of the exchange C follows a fractional power of time ($C = at^n$). An attempt has been made in this work to elucidate the role of electronic defects in the reaction mechanism from the pressure and temperature dependence of the exchange rate.

The exchange kinetics has also been studied after a deliberate introduction of electronic defects in the solid NaCl through X-irradiation and fluorination. These latter processes cause the kinetics of the reaction to change completely to a second-order rate law, and provide evidence that electronic defects are involved in the mechanism of the reaction, and that a process of absorption of a Chlorine molecule into a pair of defects is important. The mechanisms for the exchange processes use two species of electronic defect, corresponding to Seitz's models of V_2 and V_4 -Centres, and the power law ($C = at^n$) mechanism requires a transition complex between the two defects.

D. Objects of the Present Work

The general objective was to determine the mechanisms of oxidation of KI(s) by $Cl_2(g)$ and $F_2(g)$. To this end, the following types of experiments were undertaken:

(1) X-ray diffraction to characterize the reaction products

as KCl or a polyhalide;

(2) kinetic studies by chemical analysis of the I_2 produced;

(3) studies of the d.c. electrical conductivity of the solid phase. It was expected that this would be a useful method, since the mechanisms are likely to require the formation and migration of cation vacancies and positive holes, both of which should contribute to the conductivity. It is not easy to get unequivocal evidence of whether the conductivity is ionic or electronic, but it was considered useful to study polarization effects to get some indication of this (such effects can disappear at high temperatures for ionic conductivity, but their disappearance at room temperature has been taken to indicate a probable change to electronic conductivity).

The studies of conductivity undertaken were:

(a) conductivity changes during reaction, which comprise the greater part of the experimental work reported in this thesis;

(b) the conductivity of KI as a function of temperature, from room temperature up to 330° C. (The conductivity of the alkali halides has been studied extensively above about 250° C., but below that temperature a thorough study has been reported only for NaCl (28).)

EXPERIMENTAL

A. Preparation of KI Samples

Single crystals of KI, $\frac{1}{2}$ -inch diameter by 2 mm. thick, cut parallel to cleavage plane, were obtained from the Harshaw Chemical Company. For all powders and pellets, Mallinckrodt reagent grade KI was used. For pressing into pellets, the powder was loaded into the die in a dry box and evacuated to about 1μ before pressing at 8,000 p.s.i. in a Carver Hydraulic Press for 2 minutes. The following types of powder were used:

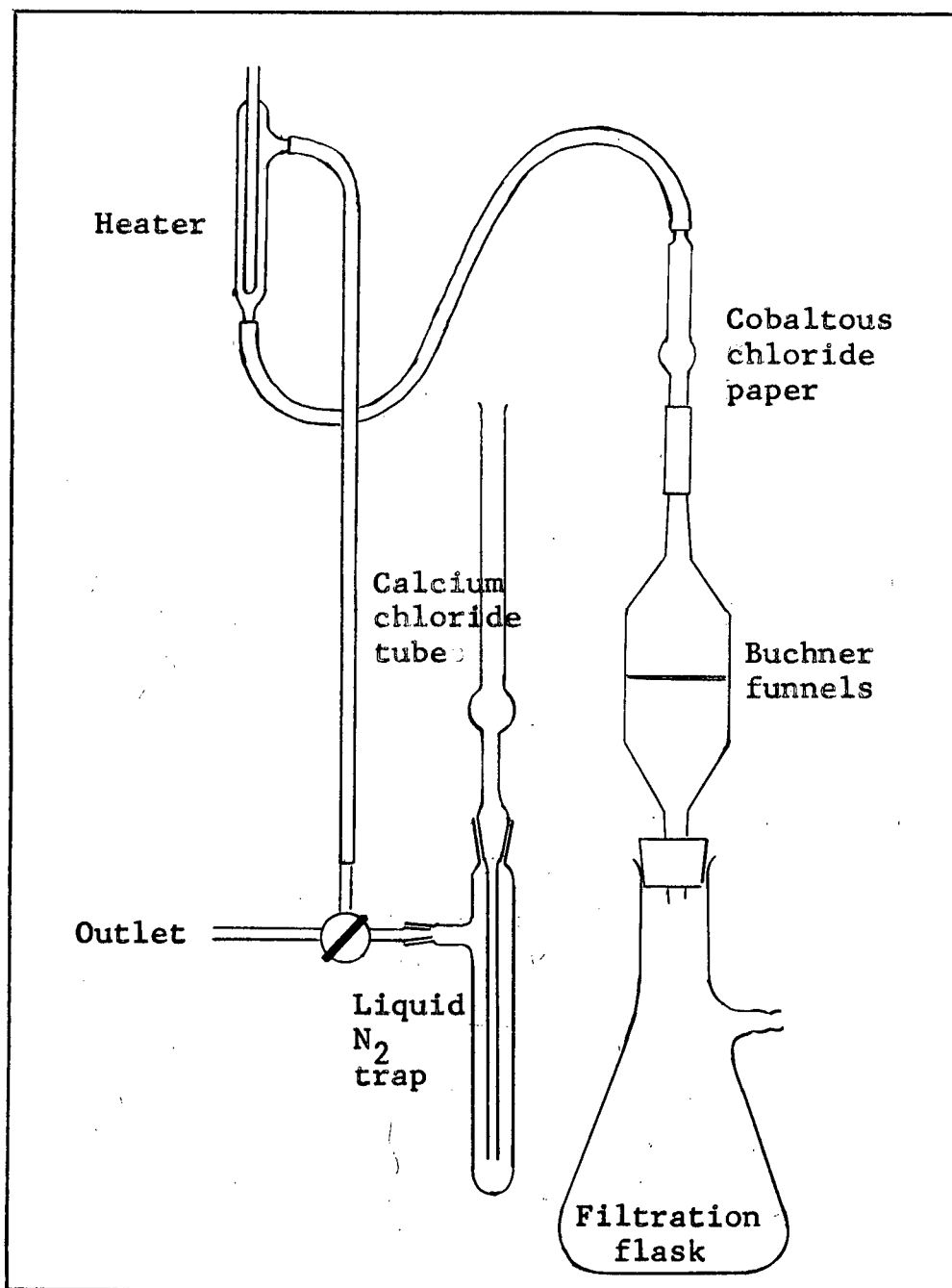
(i) "Large Particles" (size 0.05 to 0.5 mm. by microscopic examination), prepared by grinding in a mortar and oven-drying for three days at 120° C.

(ii) "Small Particles" (size 3-19 μ from surface area determination by B.E.T. method using Krypton as adsorbate), prepared by freezing 18 ml. of a saturated aqueous KI solution in liquid N_2 and mixing with 2 l. of methyl ethyl ketone. The particles were dried for an hour on the filter in a stream of $CaCl_2$ dried air, and overnight in a dry box ($< 1\%$ R.H.).

(iii) "Small Particles" similarly prepared, but with Iodine previously dissolved in the M.E.K. at 10^{-4} mole l. $^{-1}$. (For sections (ii) and (iii) see Figure 5.)

FIGURE 5

VACUUM FILTRATION APPARATUS



B. Determination of the Surface Area of Small Particles

(i) Apparatus

The adsorption apparatus was a constant volume manometric apparatus using a McLeod gauge designed to read Krypton pressures up to 1 mm. of Mercury. The Krypton used was supplied by the Air Co., specified mass spectrometrically pure. All stopcocks and joints in the system were greased with Apiezon M or T grease. The vacuum was created by a single stage Mercury diffusion pump backed by a duo-seal rotary oil pump. The cold traps were kept at liquid N₂ temperature during the adsorption runs. The Krypton storage bulb was connected by a stopcock to a burette whose capacity of about 1 cc. allowed pressures of up to 20 cm. of Hg to be manipulated.

(ii) Calculation of Surface Area

The surface area was calculated using the B.E.T. equation

$$v = V_m \cdot c \cdot p / (p_0 - p) \left[1 + (c-1) \left(\frac{p}{p_0} \right) \right] \quad (3)$$

where V_m is the volume of Krypton adsorbed at S.T.P. for a complete monolayer adsorption. c is $\exp(E_1 - E_L / R.T.)$, where E_1 is the heat of adsorption in the first layer, E_L is the

heat of liquification of the Krypton on the surface (and is assumed to be the heat of adsorption in all layers except the first). p is the equilibrium pressure after adsorption of v_{cc} and p_0 the vapour pressure of Krypton at the temperature of the experiment, i.e., -197° C. (liquid N_2 temperature).

After rearranging equation (3), one gets

$$\frac{p}{v(p_0 - p)} = \frac{1}{V_m \cdot c} + \frac{c-1}{V_m \cdot c} \frac{p}{p_0} \quad (4)$$

A plot of $p/v(p_0 - p)$ versus (p/p_0) gives a straight line if the theory is obeyed. The intercept is $(1/V_m \cdot c)$ and the slope $(c-1/V_m \cdot c)$, and thus V_m and c can be determined.

Assuming an atomic radius of 1.78 \AA for the close-packed Krypton atoms, by multiplying V_m by 2.24 one obtains the total area of the adsorbate in $\text{m}^2\text{gm.}^{-1}$. From the surface area in $\text{m}^2\text{gm.}^{-1}$, the particle size can be calculated.

C. Halogen Handling System

All operations with halogen gases in this laboratory have been confined to a single vacuum system. The vacuum was created by using a 3-stage Balzer diffusion pump containing Dow Corning 703 high vacuum Silicone fluid.

Right-angled stopcocks were used throughout the system to minimize leakage from streaking in the tap-grease

(KEL-F No. 90 grease). Sulphuric acid manometers were used throughout, operating non-linearly with some air in the closed limb, and calibrated against a Mercury manometer. A disposal line for the halogens was connected to all parts of the system. This return line (disposal line) was separate from the main vacuum line but was evacuated by the same pumps. Chlorine was usually condensed into liquid N_2 traps (and afterwards dissolved in NaOH solution), and Fluorine was absorbed in soda lime.

The vacuum in the system was usually measured by a Veeco RG.75P "ionization" gauge with a "non-burnout" Iridium filament. (It was found that the filament of these gauges is easily damaged by quite small amounts of halogen gases.) The vapour pressure of the concentrated H_2SO_4 used in the manometers was 7×10^{-4} mm. of Hg, as measured by the ionization gauge (Veeco type).

(i) Chlorine Purification System

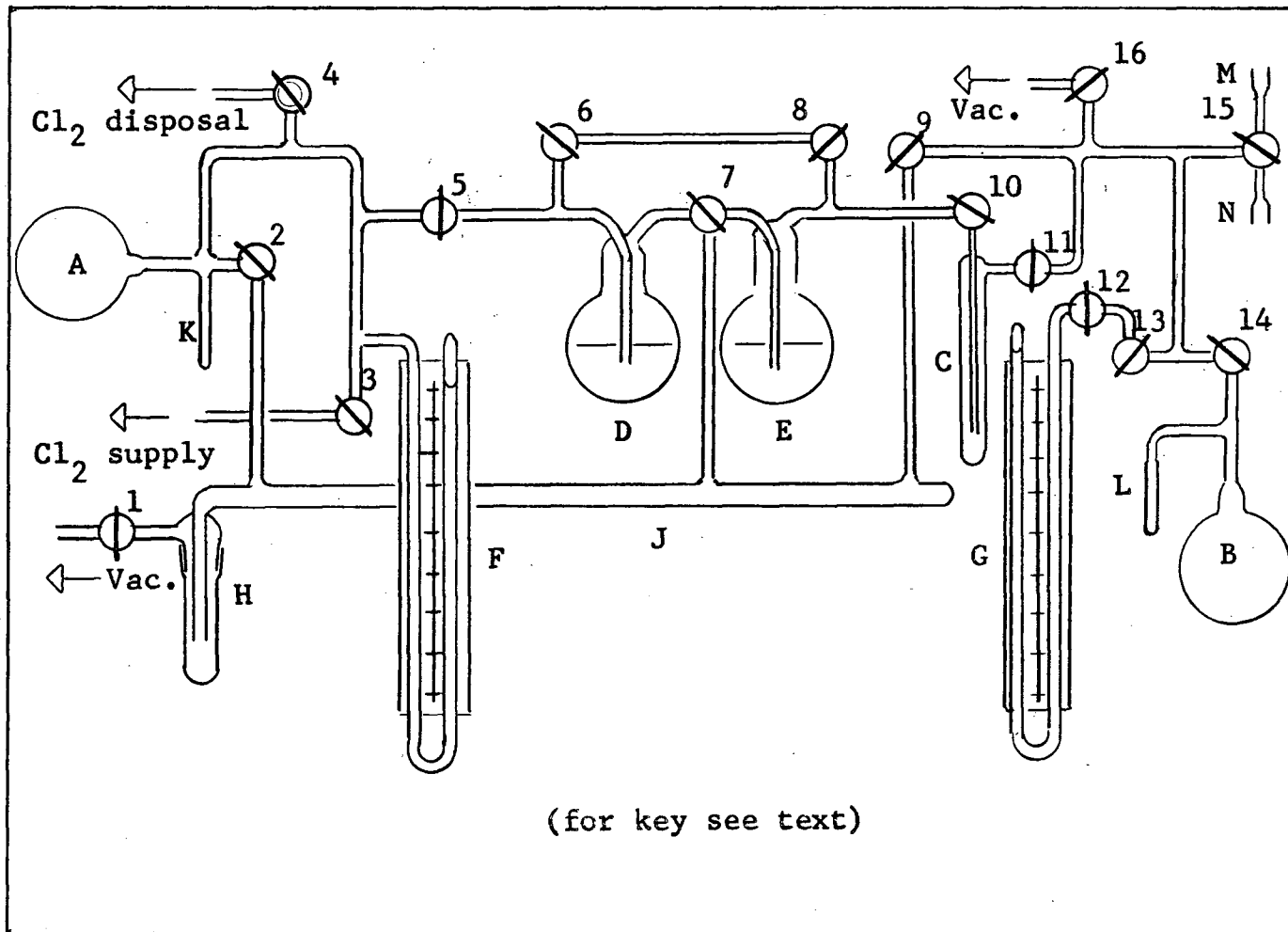
Matheson Chlorine gas (specification 99.5% pure) was used directly in some of the earlier work on product analysis and kinetics of oxidation of powders, but in most of the experiments it was purified, by the removal of non-condensable gases, and by drying with concentrated sulphuric acid. The purification apparatus is shown in Figure 6.

The disposal line (or the halogen return line) was connected to 4. D and E are wash bottles containing concentrated H_2SO_4 , and F and G are sulphuric acid manometers.

Purification procedure was as follows: Matheson Chlorine was introduced into the 2-litre bulb A, with 2, 4 and 5 being closed. In each purification run approximately 1 atmosphere of the gas was admitted. Non-condensable gases were first removed by opening 4 to the disposal line and passing the impure supply of Chlorine through 2 U tubes cooled in liquid N_2 , connected to the disposal line (not shown in Figure 6). The Chlorine gas was condensed in the first U tube, and the second U tube served as a guard trap. The Chlorine was then condensed in K, and stopcock 4 was closed.

For the removal of water vapour, wash bottles D and E and the receiver bulb B were evacuated with 6, 7, 8, 9 and 12 closed and 10, 11, 13 and 14 left open. The stopcock 5 was opened slowly and Chlorine passed through D and E and finally collected in the bulb B. When approximately half of the gas was dried, the remainder was brought across by surrounding L with a liquid N_2 trap. Stopcock 14 was finally closed, and storage bulb B contained the supply of purified Chlorine.

FIGURE 6 - CHLORINE PURIFICATION SYSTEM



(ii) Fluorine Handling System

Matheson Fluorine gas at 300 p.s.i. (specification 98% pure) was dispensed by reducing its pressure in three successive expansions at a series of monel needle valves connected by a few feet of high pressure 3/8-inch copper tubing.

The storage bulb (volume - 1 litre) and the supply line were evacuated by a rotary oil pump (pressure checked by a tesla coil discharge). The Fluorine gas was admitted directly to the storage bulb at a pressure of the order of 1 atmosphere (measured on a helicoid test gauge). Samples of Fluorine gas were drawn from this storage bulb (using the main halogen handling system) into small bulbs (10, 15, 30 cc.) for different experiments.

The monel metal to copper couplings were backed by teflon sleeve rings. KEL-F No. 90 high vacuum grease was used for all ground glass joints.

D. Measurement of D.C. Electrical Conductivity

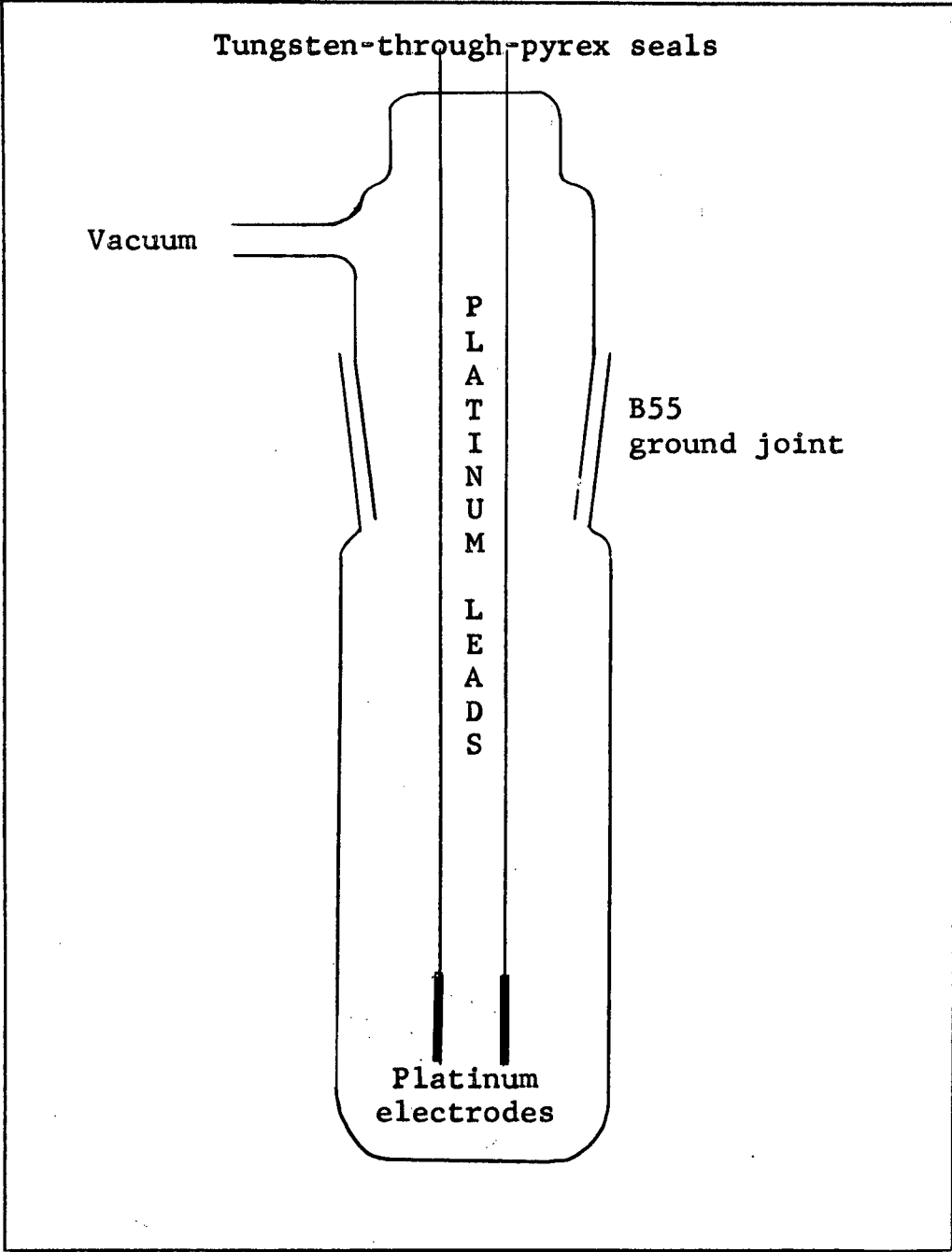
(i) Conductivity Cells

Two designs X, Y of the conductivity cells were used.

Conductivity Cell X (see Figure 7)

In this cell the electrodes were circular pieces of bright thin platinum foil. The electrode assembly was housed

FIGURE 7
CONDUCTIVITY CELL X



in a glass vessel (volume 500 ml.) forming part of the high vacuum system, with platinum leads spot-welded to tungsten-through-pyrex seals. The electrodes were held to the KI pellet by a Quickfit nickel-plated spring clamp with a 3 mm. thick sheet of Lucite on each jaw.

Conductivity Cell Y (see Figures 8, 9)

In cell Y also, the electrodes A, B were of bright thin platinum foil. The bottom electrode B was slightly smaller than the pellet and was surrounded by a concentric guard ring C, so that bulk and edge conductivity could be measured separately (see Figure 9). The electrodes were recessed into teflon supports D, E, and the whole arrangement was placed under a weight F consisting of lead shot sealed into a glass vessel. A glass cross bar G and glass hook H ensured that the weight was not supported on the leads when the outer envelope I was removed. The leads J, K, L were of platinum (spot-welded to tungsten-through-pyrex seals at the top) and were jacketed in glass. M is a Pt-10% Rh lead enabling the bottom electrode to be used as a thermocouple.

(ii) Electronic Equipment and Circuits

The cell was wired in series with a Keithley decade shunt having resistances from 10^3 ohm to 10^{12} ohm, and a P.D. of about 3 V. was applied across the whole arrangement by means

FIGURE 8
CONDUCTIVITY CELL Y

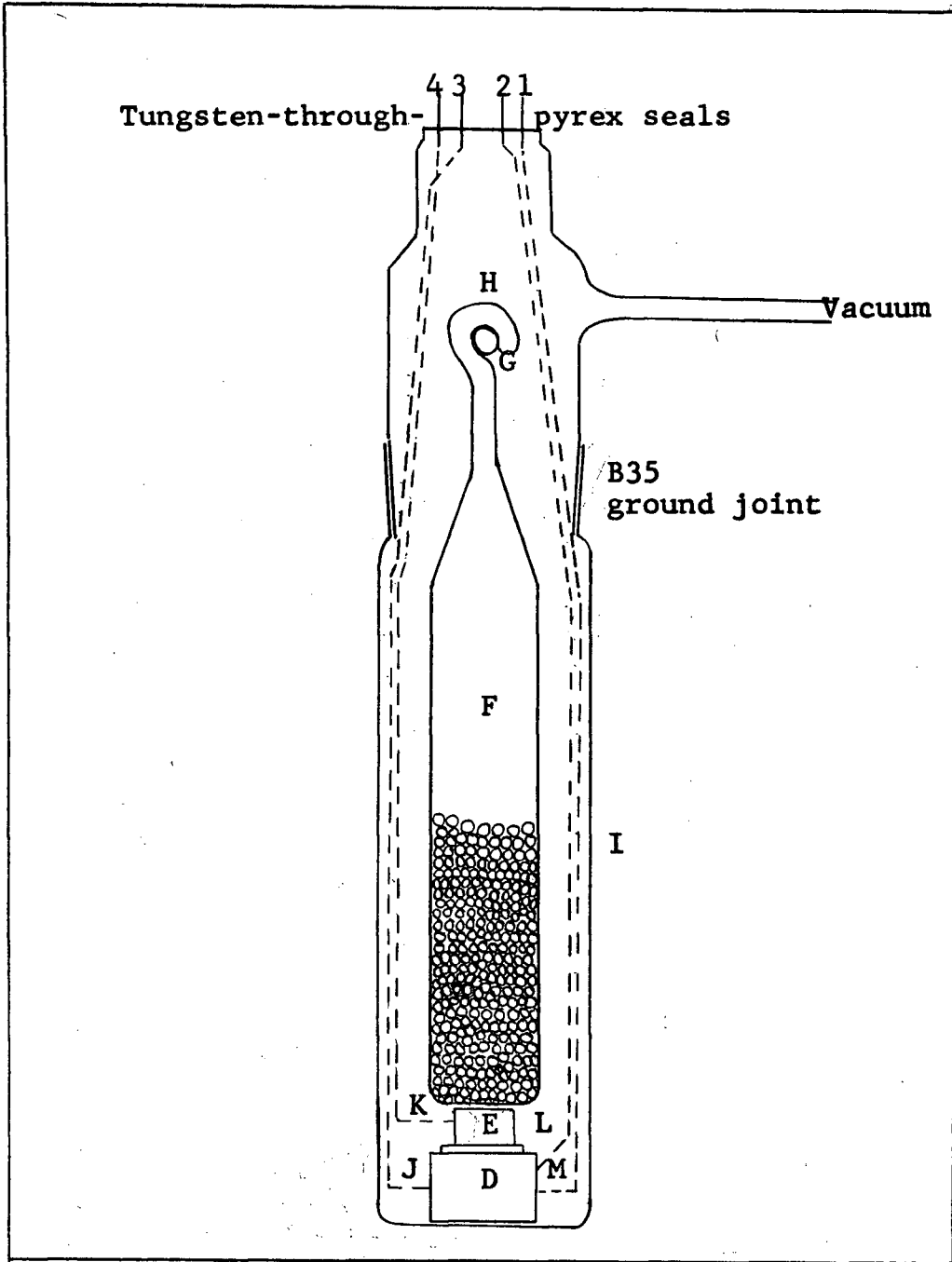
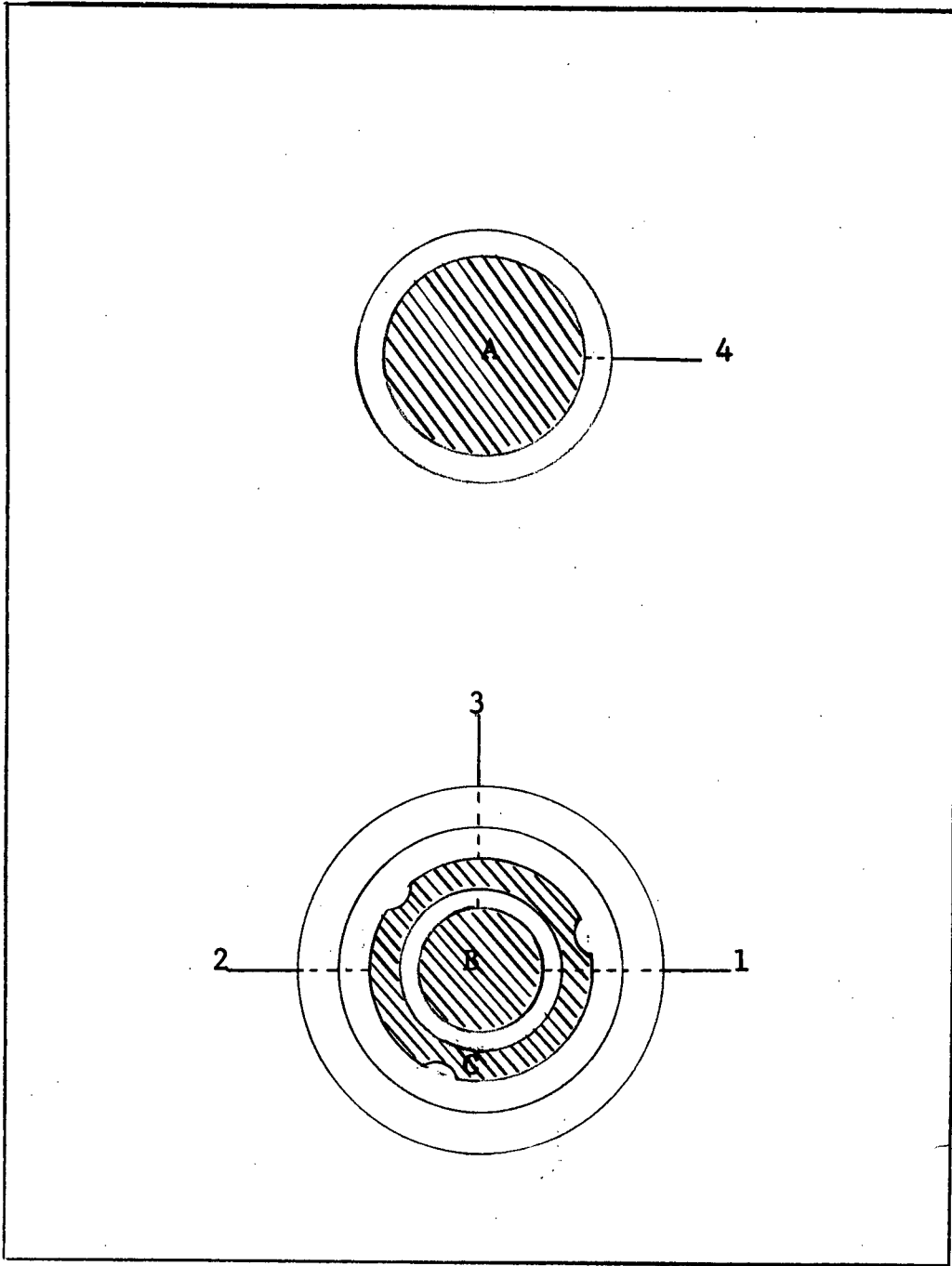


FIGURE 9
GUARD RING ARRANGEMENT



of dry cells (see Figure 10). Nearly all of this P.D. was across the pellet, that across the shunt being usually less than 80 mV. This was measured with a Keithley model 200B battery-operated electrometer (d.c. VtVm) having an input resistance of 10^{14} ohm, residual current at input 5×10^{-14} amp., and ranges down to 8 mV. full scale deflection. A switch gear (see Figure 11) was designed to permit the following operations:

- (1) reversal of applied P.D. across the sample;
- (2) use of the bottom electrode as a thermocouple (selector switch, position 1);
- (3) measurement of total applied P.D. E_1 (selector switch, position 2);
- (4) measurement of P.D. across shunt with either the bottom electrode or the guard ring or both in circuit, either part being grounded when not in circuit (selector switch, positions 3, 4 and 5).

The leads used were mainly single-conductor coaxial cables. In a large part of the work, a four-conductor cable was used between switch gear and cell Y. This was later replaced by four separate cables housed in a grounded metal conduit. The cells were covered with grounded aluminum foil. Leakage resistances limited the measurements to a maximum resistance

CIRCUIT DIAGRAM FOR THE PROCEDURE

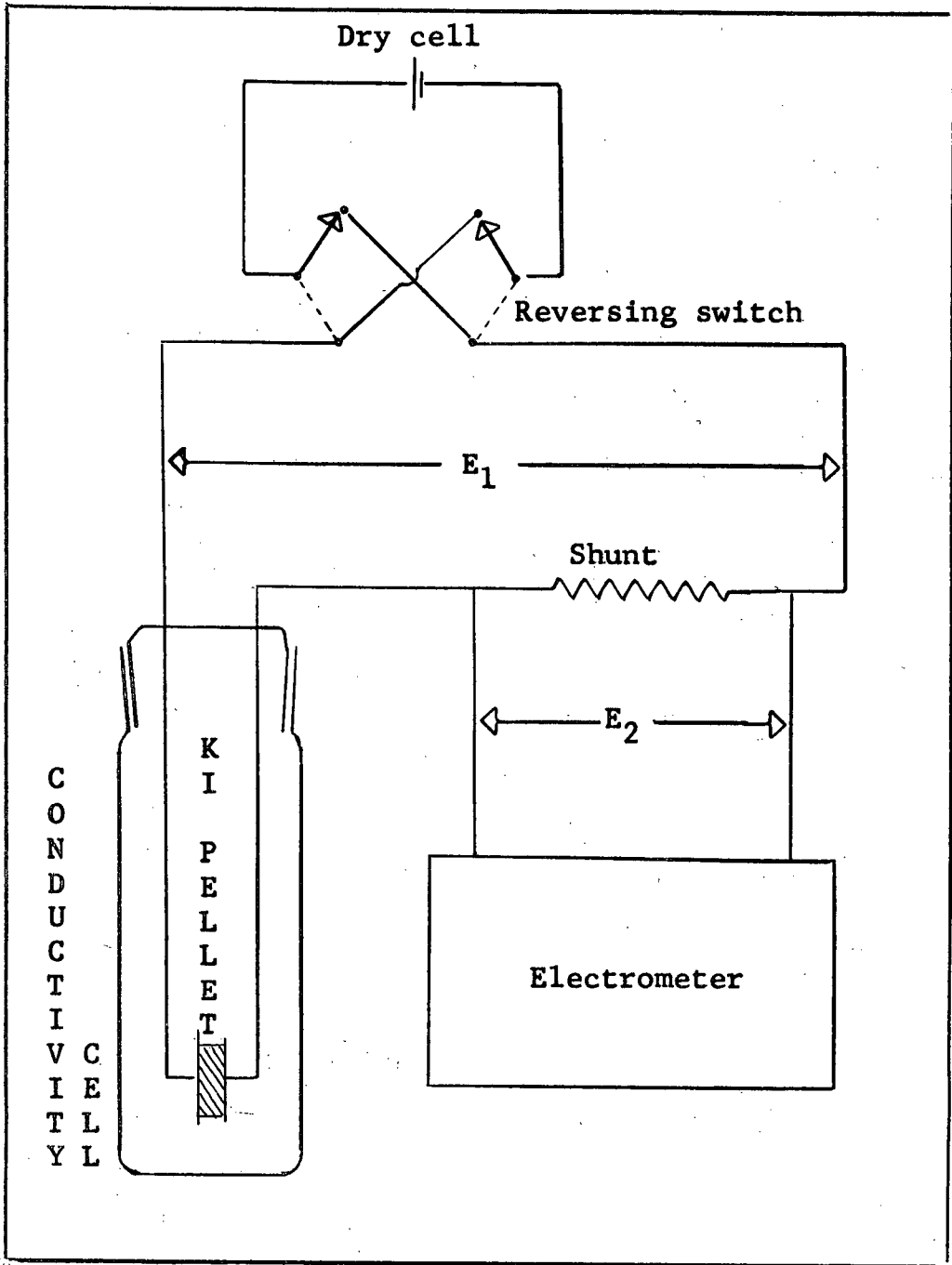
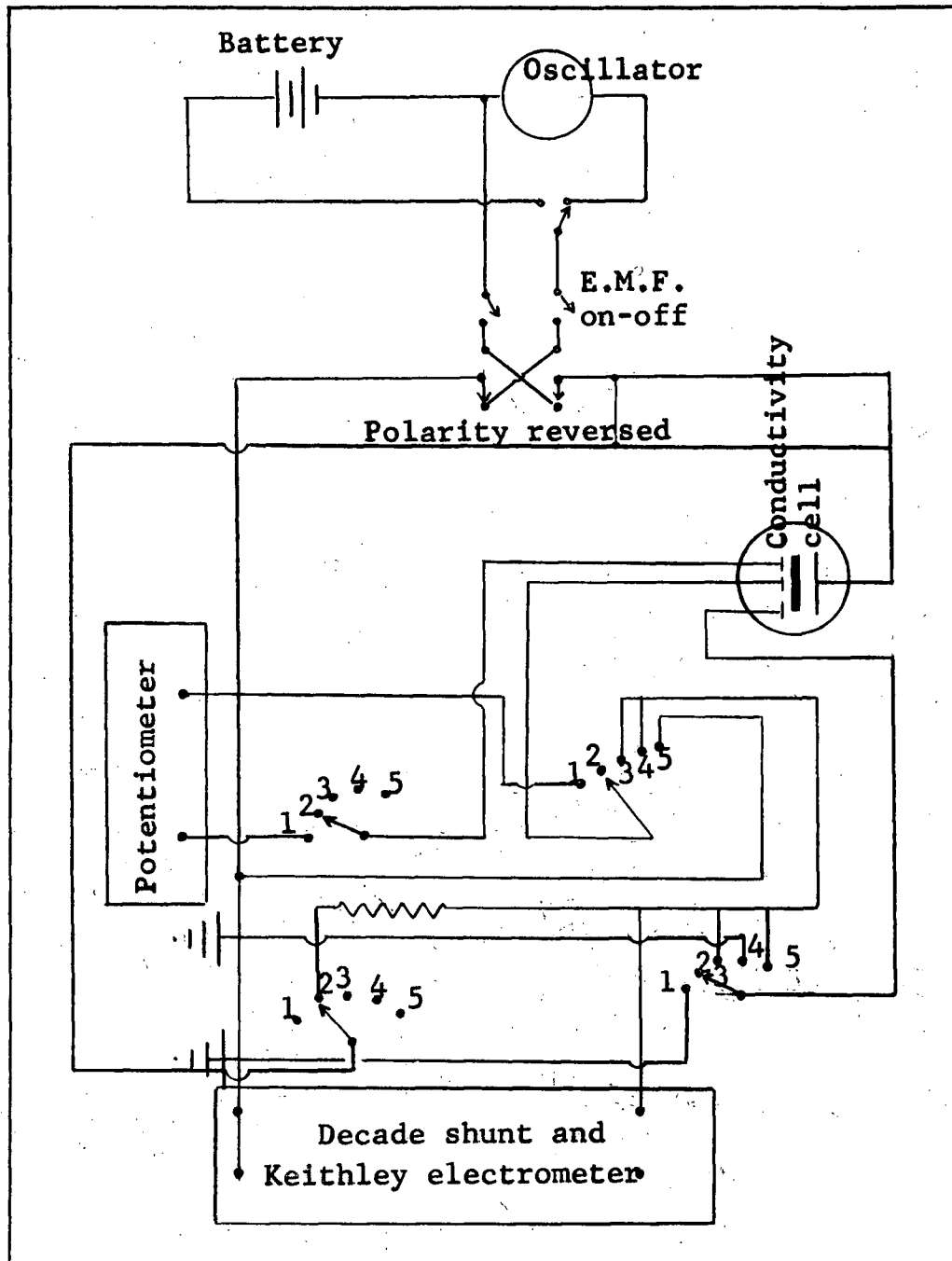


FIGURE 11
CIRCUIT DIAGRAM FOR THE SWITCH GEAR



in the sample of about 10^{13} ohm, and disturbances from moving objects near to the apparatus were noticeable at about the same value.

(iii) Procedure (refer to Figure 10)

E_1 was measured at the start of each day's measurements, and checked at intervals of 4 hours. For cell Y, E_2 was usually measured with both bottom electrode and guard ring in circuit (selector switch, position 3). The applied P.D. was usually reversed every five minutes, and E_2 was taken as the mean of the values immediately before and after reversal of E. This procedure should give a figure equivalent to that obtained by taking a reading immediately after applying the E.M.F. E_1 to an unpolarized specimen. The conductivity was then calculated as follows:

$$C = \frac{E_2}{E_1 - E_2} (I) \text{ ohm}^{-1}$$

where C is the conductance in ohm^{-1} , and I is the current range in amp. (i.e. the reciprocal of the shunt resistance).

The specific conductance was calculated with the following formula:

$$C = C_{sp} \frac{A}{l}$$

$$\text{or } C_{sp} = C \frac{l}{A} \text{ ohm}^{-1} \text{ cm.}^{-1}$$

(where l is the thickness of the sample, and A is the area, πr^2). The diameter of the pellets was 0.5".

The polarization effects were studied in order to get some indication of whether the additional conductance during the course of reaction was ionic or electronic. The quantity used as a measure of polarization was the apparent change in the conductance on reversing polarity divided by the mean conductance (i.e. the change in E_2 divided by the mean value, $\Delta E_2/E_2$). The polarization was usually reversible and reproducible, although there were occasionally rapid polarization effects (as observed by earlier workers (50,51)), which prevented accurate measurements. Most usually, individual measurements of conductance varied within a range of $\pm 10\%$ of mean, and the standard error of a dozen measurements in a one-hour period was 2%.

In making measurements on pressed pellets of KI, it was first necessary to degas the pellet in a high vacuum until its resistance had become constant. This often took up to three or four days and involved increases in resistance of factors of 10^2 to 10^4 . Thereafter, the changes in resistance during reaction with Cl_2 or F_2 could be followed sometimes for as long as several weeks. The measurements made during the first hour of any day's work were often found to be unreliable,

showing a rapid drift of the resistance with very large polarization effects (see Table I).

(iv) Determination of Conductivity as a Function of Temperature

The conductivity of the KI pellet in an atmosphere of N_2 gas was studied from room temperature (22° C. approx.) to 330° C. The purpose of the atmosphere of N_2 was to ensure rapid thermal equilibration. In the set-up the conductivity cell Y was first covered with aluminum foil and then grounded. It was then surrounded by a simple furnace with a 30-ohm nichrome winding supported on a heavy copper tube, with asbestos insulation. The entire system was shielded by aluminum foil which was grounded. It was also necessary to ground the copper tube to prevent serious interference from the alternating current in the heating coil. The furnace was supplied with a variable voltage 0-110 V., by a $7\frac{1}{2}$ amp. Variac. Its maximum temperature was 330° C. A portable Honeywell potentiometer model no. 2732 was used for measurement of the E.M.F. of the Pt vs. Pt-10% Rh thermocouple in the cell. The procedure for the measurement of conductivity was the same as outlined in section (iii).

For the temperature measurement, the selector switch (switch gear) was returned to position 1 (thermocouple) and

TABLE 1

EXTRACT FROM THE LABORATORY DIARY

Measurements during reaction of a KI pellet with Cl_2 ; run S II at 115 hoursCurrent range 10^{-5} amp. $E_1 = 3.20$ volts

Time (min.)	Polarity	E_2 (V)	ΔE_2 (V)	Polarization (f)	$\left(\frac{E_2}{E_1 - E_2} \times \text{current range}\right)$ $= C(\text{ohm}^{-1})$	C_{sp} (ohm^{-1} cm.^{-1})
0	+	0.00368				$\times 10^{-9}$
5		0.00194				
5.1	-	0.00344	0.00269	0.00150	0.557	8.41
10		0.00180				8.57
10.1	+	0.00378	0.00279	0.00198	0.710	8.72
15		0.00195				
15.1	-	0.00350	0.00273	0.00155	0.568	8.54
20		0.00182				8.53
20.1	+	0.00362	0.00272	0.00180	0.662	8.51
25		0.00200				
25.1	-	0.00342	0.00271	0.00142	0.524	8.47
30		0.00152				8.22
30.1	+	0.00358	0.00255	0.00206	0.810	7.97
35		0.00195				
35.1	-	0.00360	0.00278	0.00165	0.594	8.69
40		0.00200				8.88
40.1	+	0.00380	0.00290	0.00180	0.620	9.06
45		0.00218				
45.1	-	0.00384	0.00301	0.00166	0.552	9.41
50		0.00220				9.60
50.1	+	0.00406	0.00313	0.00186	0.594	9.79

the E.M.F. recorded through the potentiometer. The corresponding temperature was found by consulting standard tables on Pt vs. Pt-10% Rh thermocouples. Since all the junctions were at room temperature, room temperature was added to the readings obtained from the potentiometer.

Each conductivity reading was taken after thermal equilibrium had established in the system (usually after about 2 hours).

E. Analysis of Reaction Products

(i) Characterization of the Reaction Products by X-Ray Diffraction

Qualitative analysis of reacted powders was carried out by Debye-Scherrer X-ray powder photography in a 14.3 cm. camera with nickel-filtered copper radiation. Samples of reagent grade KI were ground in a mortar, loaded into 0.5 mm. capillary tubes, outgassed for a short time in a high vacuum system (10^{-6} mm. Hg), and reacted with Chlorine gas at 512 mm. Hg and room temperature. The capillaries were sealed off immediately after removal from the vacuum system. To obtain a powder photograph of $KICl_2$, the compound was prepared similarly from KCl and ICl vapour. Lines to be expected in the diffraction pattern of $KICl_4$ were calculated from its

known unit cell dimensions.

(ii) Determination of Iodine by Volumetric Analysis

Quantitative work on the kinetics of formation of Iodine was carried out on similar powdered samples of about 1 gm. KI, exposed to Chlorine at the same pressure (512 mm. Hg) and room temperature for periods up to several days. Each sample was dissolved in water (rapidly, to avoid sublimation of Iodine), made up to 100 ml., and 25 ml. portions were titrated against 0.01 N $\text{Na}_2\text{S}_2\text{O}_3$ with starch indicator. A similar method could not be used for pressed pellets, since the Iodine was present in very small quantity and volatilized very rapidly on exposure to the atmosphere.

(iii) Determination of Halide Ions by Potentiometric Titration

Attempts were made to estimate the relative amounts of chloride and iodide ions by potentiometric titration with AgNO_3 , with a silver electrode combined with a glass electrode as reference using Beckman Zeromatic pH meter. 2 ml. of 0.5 M $\text{Ba}(\text{NO}_3)_2$ solution was added to a 10 ml. solution of the mixture of halides to prevent co-precipitation. The method was sufficiently sensitive to detect an extent of reaction of 1%.

RESULTS

A. Study of Reaction Products & Kinetics (KI/Cl₂ System)

(i) X-Ray Diffraction (Powdered Samples)

X-ray powder photography indicated KCl and I₂ as the only products of the reaction of KI and Cl₂ at 512 mm. Hg and room temperature for periods up to 9 days. The lattices of KICl₄ and KICl₂ were not found in any sample. A yellow colour appeared only once in a minute fraction of one sample and this result could not be reproduced.

(ii) Kinetics (Powdered Samples)

Calculation of % KI Oxidized (Reacted)



2 moles KCl are formed for every mole I₂

Final wt. of KI = Total wt. KI - wt. I₂ - wt. KCl

Original KI (moles) = Final KI (moles) + 2 x moles I₂

$$\% \text{ KI oxidized (reacted) } = \frac{2 \times \text{moles I}_2}{\text{original KI (moles)}} \times 100$$

Sample Calculation for KI Sample Reacted for 9 Days

Amount of I₂ determined (volumetrically) = 3.0×10^{-2} M.

wt. of I₂ = 3.0×10^{-2} x 254 gms.

and wt. of KCl = 3.0×10^{-2} x 74.6 x 2 gms.

Final wt. of KI = 166 - 3.0×10^{-2} x 254 - 3.0×10^{-2} x 149.2 gms.
 = 166 - 3.0×10^{-2} (254 + 149.2) gms.

$$= 166 - (3.0 \times 403.2) \times 10^{-2} \text{ gms.}$$

$$= 166 - 12.09$$

$$= 153.91$$

$$\text{Original wt. of KI} = \frac{153.91}{166} + 6 \times 10^{-2} = 98.76 \times 10^{-2} \text{ moles}$$

$$\% \text{ KI oxidized} = \frac{2 \times 3 \times 10^{-2}}{98.76 \times 10^{-2}} \times 100 \approx 6 \%$$

(For complete results see Table 6 in the Appendix.)

The kinetic results, based on analysis for Iodine (as outlined above), are shown in Figure 12, in which every point represents an average of from two to four samples. They indicate the reaction is zero-order up to at least 9 days, when 6% of the KI has been oxidized.

(iii) Potentiometric Determination of Halide Ions (Pressed Pellets)

The Iodine present in the reacted pellet was in very small quantity, and volatilized away very rapidly on exposure to the atmosphere. Attempts to estimate the relative amounts of Chloride and Iodide ions by potentiometric titration gave negative results for Chloride in a pellet which appeared to have reacted to the greatest extent of all pellets studied (see Figure 13).

FIGURE 12

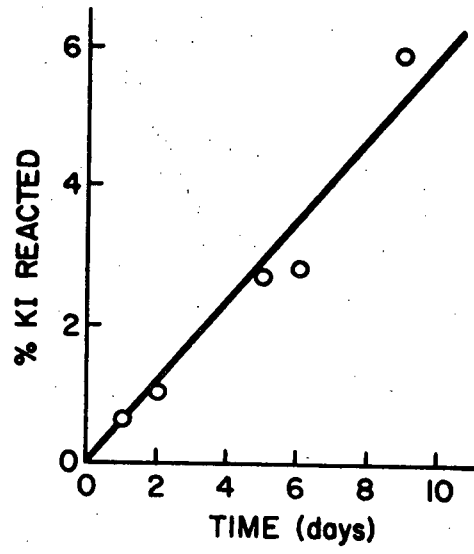
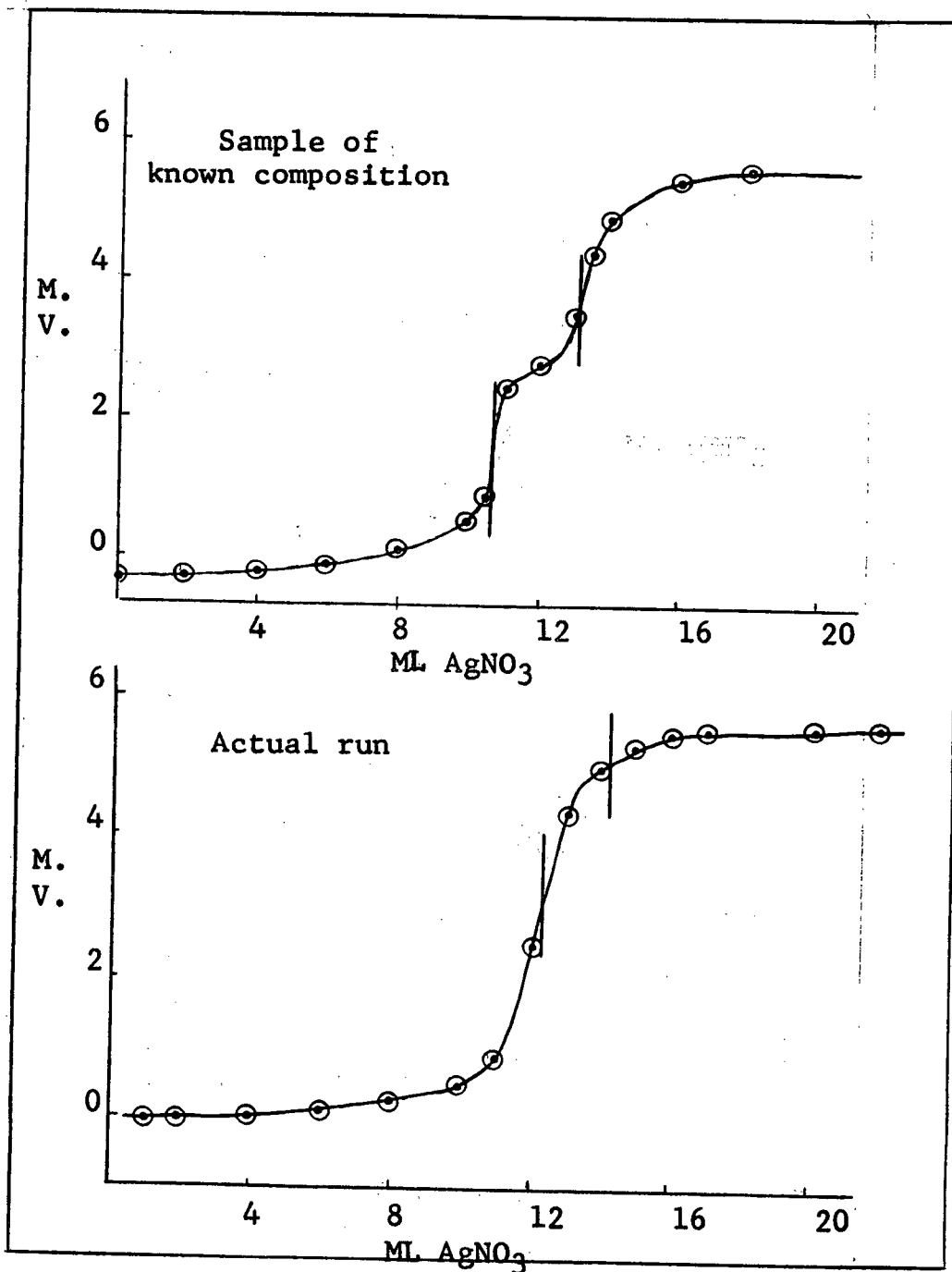
REACTION OF POWDERED KI WITH Cl_2 ; ZERO-ORDER PLOT

FIGURE 13

POTENTIOMETRIC TITRATION CURVES



B. The Electrical Conductivity of Pure KI

(i) Room Temperature Conductivity

In strong contrast to the results of Dreyfus and Nowick (28) for NaCl, the conductivity of my KI samples at room temperature was very variable (10^{-12} to 10^{-7} ohm⁻¹ cm.⁻¹, see Table 7 in the Appendix), and always enormously greater than that found by extrapolating the impurity range (50) from 250° C. down to room temperature, which gives C_0 as 10^{-16} ohm⁻¹ cm.⁻¹. To try to determine the precise conditions for obtaining high or low conductivity pellets, the conductance at room temperature of various types of preparation of KI was determined, as shown in Table 2, on the following page.

These results appear to indicate that small particles which are "badly" prepared (in the sense of poor drying conditions and no evacuation before pressing) have low conductivity, comparable to that of a good single crystal or fused sample. On the other hand, as the conditions of handling of the small particles improve (lower R.H., longer drying period, evacuation before pressing), the value of C_0 becomes more variable and is often very high.

TABLE 2

INITIAL CONDUCTIVITY OF VARIOUS SAMPLES OF KI AT 23° C.

Type of KI Sample	$10^{11} C_0$ ohm ⁻¹ cm. ⁻¹
Single crystal (Harshaw)	1.85
Fused and mortar-ground sample	3.28
Fused, mortar-ground, CdI ₂ doped (1%)	2.14
Small particles, dried 4% R.H. 18 hr., not evacuated	0.85
Small particles, dried 0% R.H. 18 hr., not evacuated	1.37 to 10.85
Small particles, dried 0% R.H. 18 hr., evacuated *	0.13 to 11,000
Small particles, dried 0% R.H. 60 hr., evacuated	698

* The samples used in many of the reactions with Cl₂
(see Table 7 in the Appendix).

Polarization effects in the pure KI pellets have been studied at room temperature in order to get some indication whether the enhanced conductivity in the halogenated samples was ionic or electronic. For pure KI samples this quantity was usually in the range 0.3 to 1.73 (see Table 12 in the Appendix), and was steady over long periods in any one pellet although it

varied widely from one pellet to another.

(ii) Conductivity as a Function of Temperature

Experiments on the conductivity of KI as a function of temperature were undertaken to investigate further the discrepancy between my room temperature measurements and extrapolation of Lehfeldt's (50) results. The temperature dependence of the electrical conductivity of KI in the temperature range 250°-680° C. was determined by Lehfeldt (50). In this work I have tried to study the low temperature (22° C. - 330° C.) dependence of the electrical conductivity of KI. Plots of $\log C$ (where C is the conductivity) against $1/T$ have been made both for Lehfeldt's results (an enlargement of the plot in his paper) and for my results (see Figures 14, 15, and Tables 8, 9 Appendix). The activation energies for the different regions of the plots were determined from the slopes of the plots. The results are shown in Table 3, on the following page.

Five different runs were made for the temperature rising and falling data. In each case two different regions were observed with a break at a low temperature (see Table 4). The activation energies calculated in the first region (low temperature) were always small compared to the second region (high temperature region). As the temperature was rising continuously in the other runs (runs other than the one

FIGURE 14

ELECTRICAL CONDUCTIVITY OF KI, 250° C. TO 680° C. (LEHFELDT)

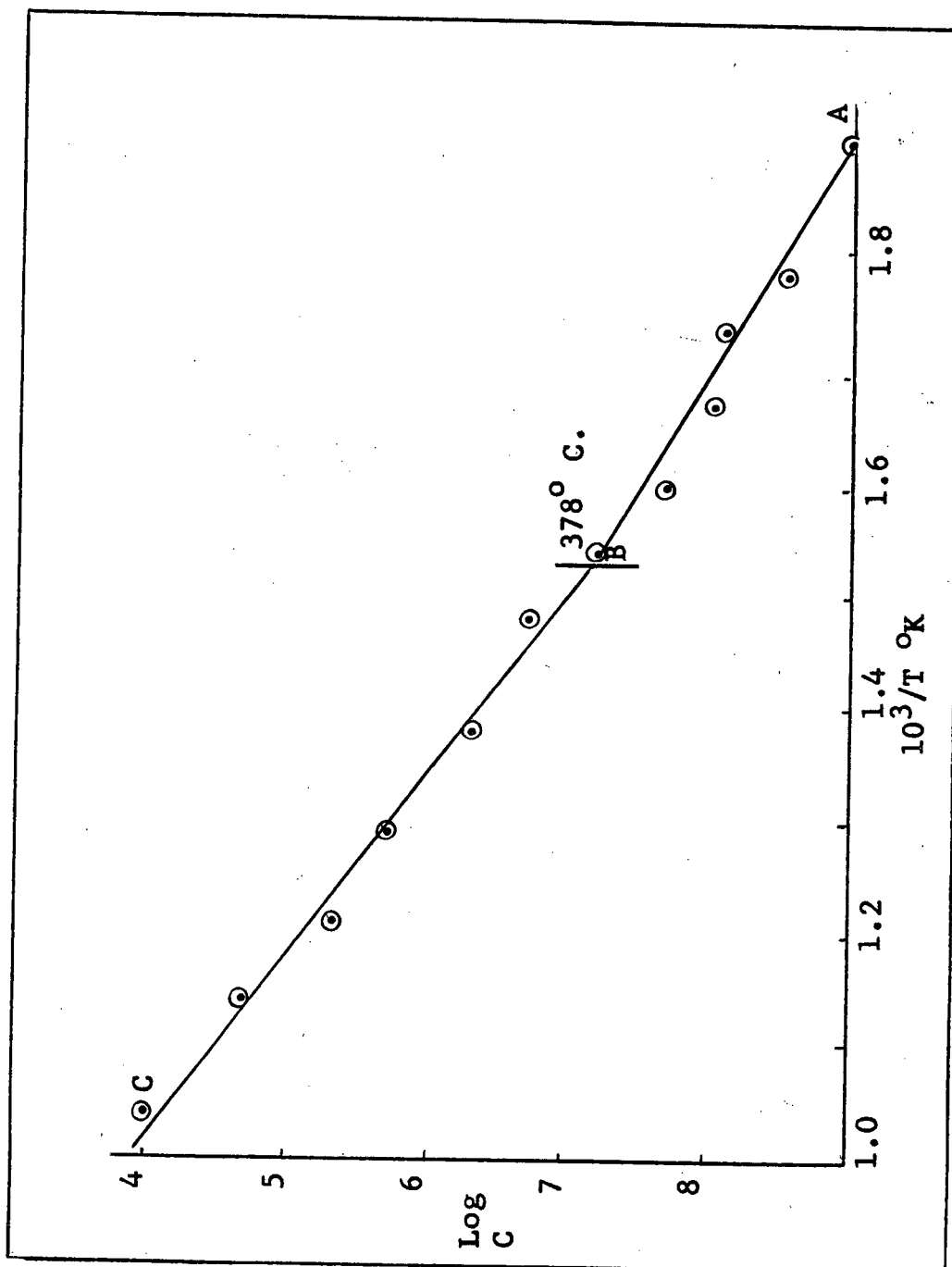


FIGURE 15

ELECTRICAL CONDUCTIVITY OF KI, 22° C. TO 330° C. (THIS WORK)

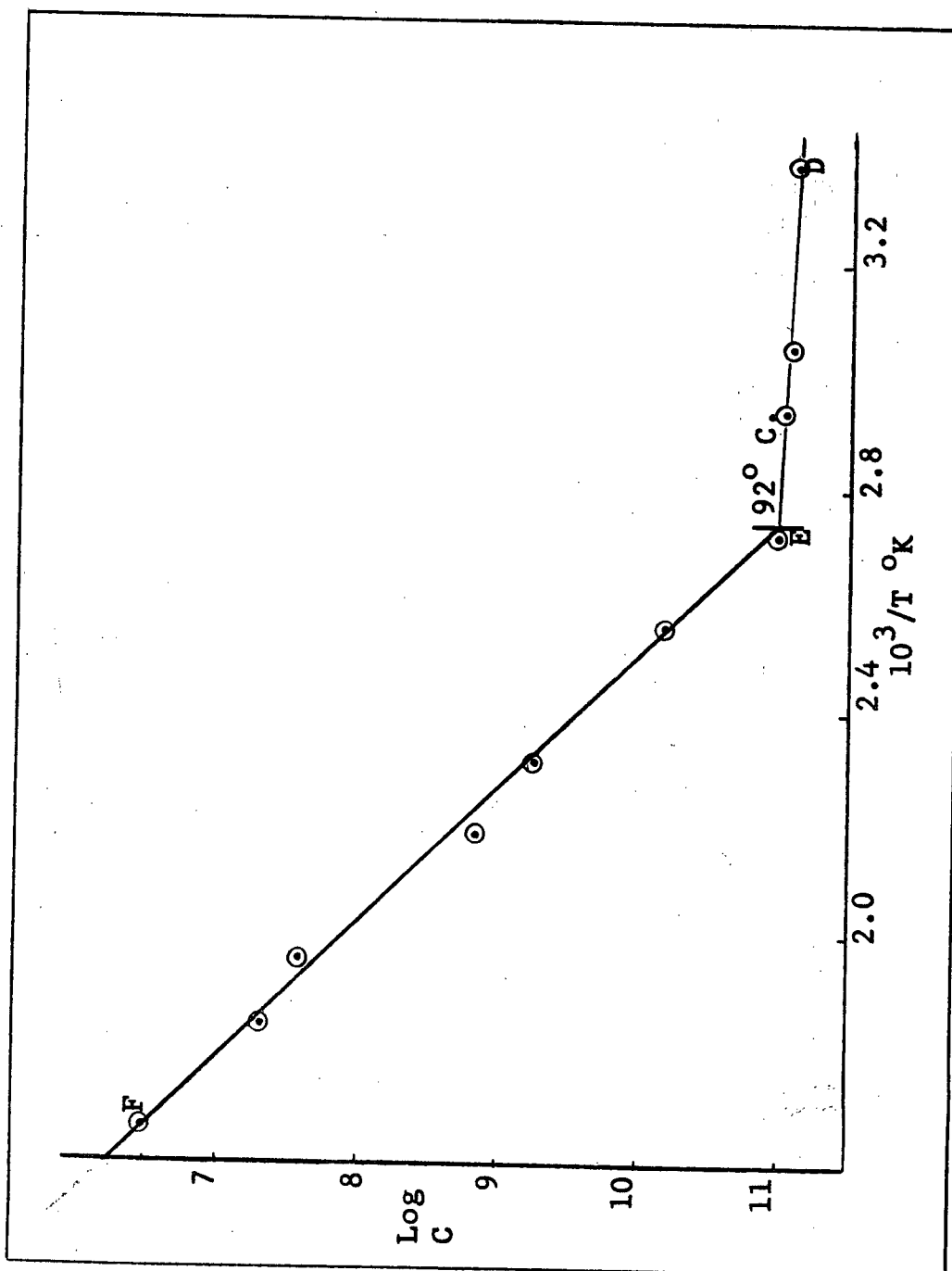


TABLE 3

ACTIVATION ENERGIES OF THE ELECTRICAL CONDUCTIVITY OF KI

Reference	Region in Fig. 14	Temperature range	E_a (eV.)	Type of material
Lehfeldt	BC	(378-680) ^o C.	1.77	Single crystal
Phipps & Partridge			1.61 (52)	Pressed pellet
Lehfeldt	AB	(250-378) ^o C.	0.822	Single crystal
	Fig. 15			
This work	EF	(92-330) ^o C.	0.817	Pressed pellets
	DE	(22- 92) ^o C.	0.016	

reported), no quantitative estimates of the activation energies were possible. The run reported in Table 4 is the most reliable one, because the readings were taken after thermal equilibrium had been established in the system. From these five runs it is clear that the temperature of the first break is sensitive to the size of the particle used in pressed pellets; this result is illustrated in Table 4.

TABLE 4
CORRELATION OF PARTICLE TYPE WITH TEMPERATURE OF
FIRST-BREAK IN LOG C vs. 1/T CURVE

No. Run	Type of Particle	Temperature of First-Break in ° C.
1	large	127
2	large	92
3	large	120
4	small	154
5	small	159

The absolute value of the conductivity at 300° C. is $1 \times 10^{-8} \text{ ohm}^{-1} \text{ cm.}^{-1}$ according to Lehfeldt's results, and $3.18 \times 10^{-7} \text{ ohm}^{-1} \text{ cm.}^{-1}$ according to my results. This discrepancy in the conductivity results is most probably connected with the purity of the sample. The purity of my sample is given in Table 10 (Appendix), but the purity of Lehfeldt's samples is not known.

C. Changes of Electrical Conductivity during Reaction of KI Samples (Pressed Pellets) with $\text{Cl}_2(\text{g})$ or $\text{F}_2(\text{g})$

(i) Types of Reaction

The processes occurring within the first few days of the halogenation of KI samples entailed large and readily measurable changes in conductivity. These changes always commenced with an increase in conductivity during the first few hours. Thereafter two clearly distinguished types of behaviour were observed in different experiments. They have been designated as types A and B. Type A behaviour is a slow decay of the conductance back to a value close to its original value (see Figure 16). Type B behaviour is a second rise in conductivity accelerating in a manner characteristic of reactions involving nucleation of a new solid phase (see Figure 16). The type of behaviour (A or B) is determined by the initial conductance C_0 of the pellet, as indicated in Table 5. In the KI/Cl_2 system both types of behaviour were observed, although type B is rather uncommon; but in the KI/F_2 system type B only has been observed. (The symbols C and C_∞ in the following account represent conductivity in excess of C_0 .)

(ii) Type A Reactions

As mentioned previously, the type A behaviour is a

FIGURE 16

REACTION OF PRESSED PELLETS WITH Cl_2 ;

CONDUCTIVITY AND POLARIZATION IN TYPE A AND TYPE B BEHAVIOUR

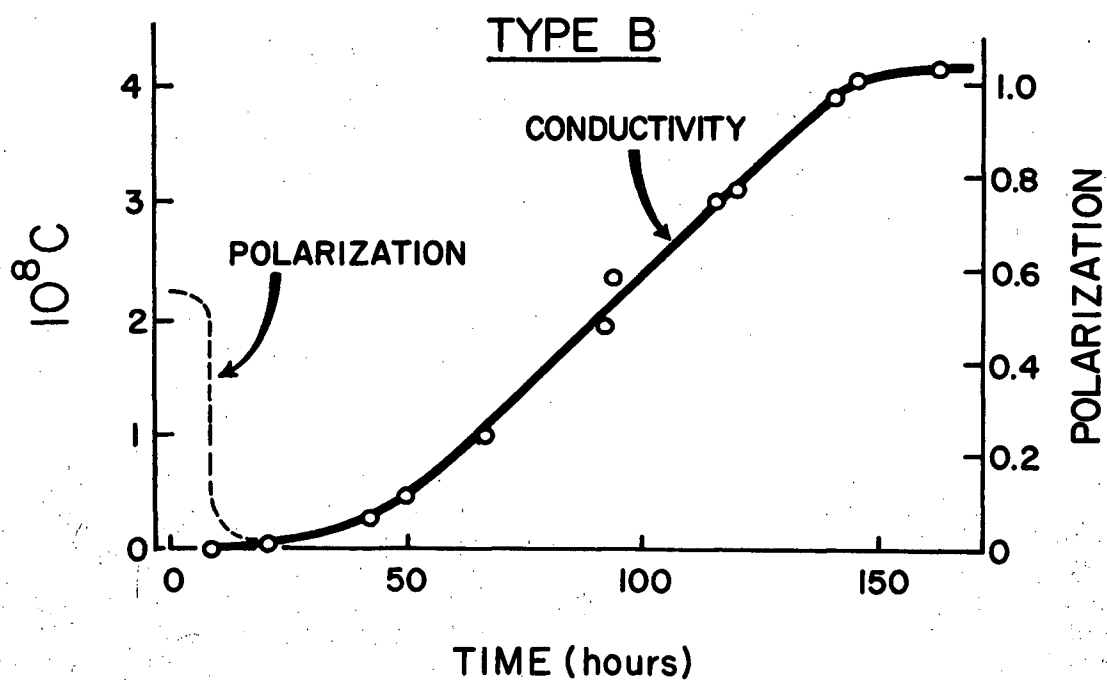
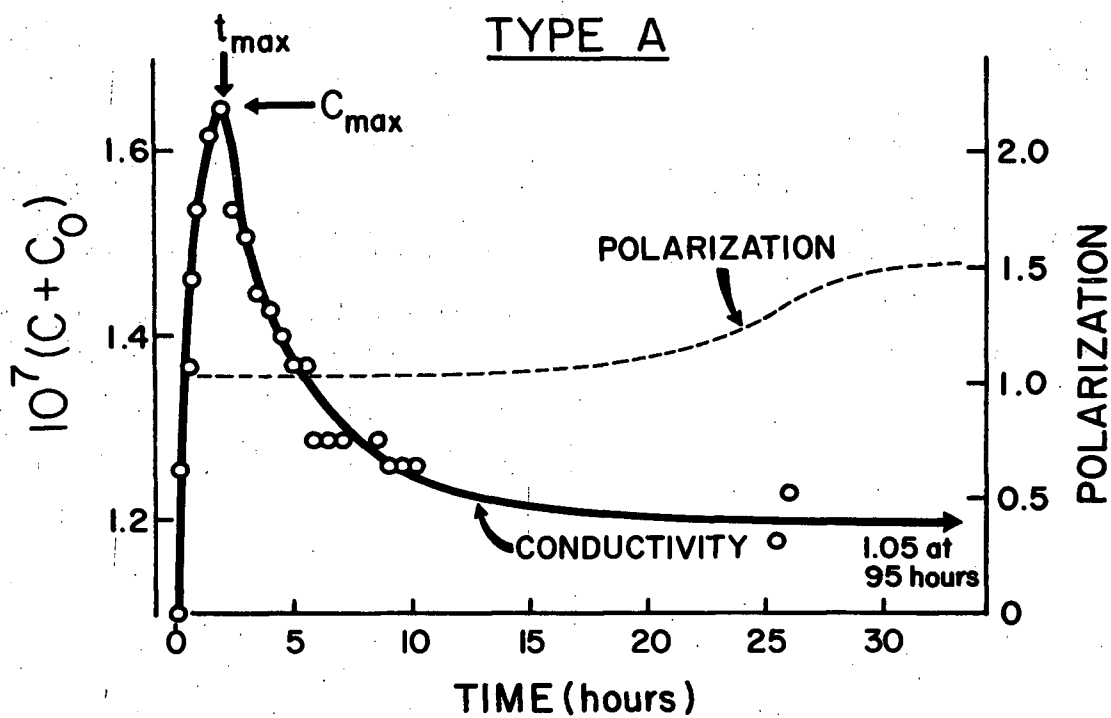


TABLE 5

BEHAVIOUR AFTER INITIAL RISE IN CONDUCTANCE

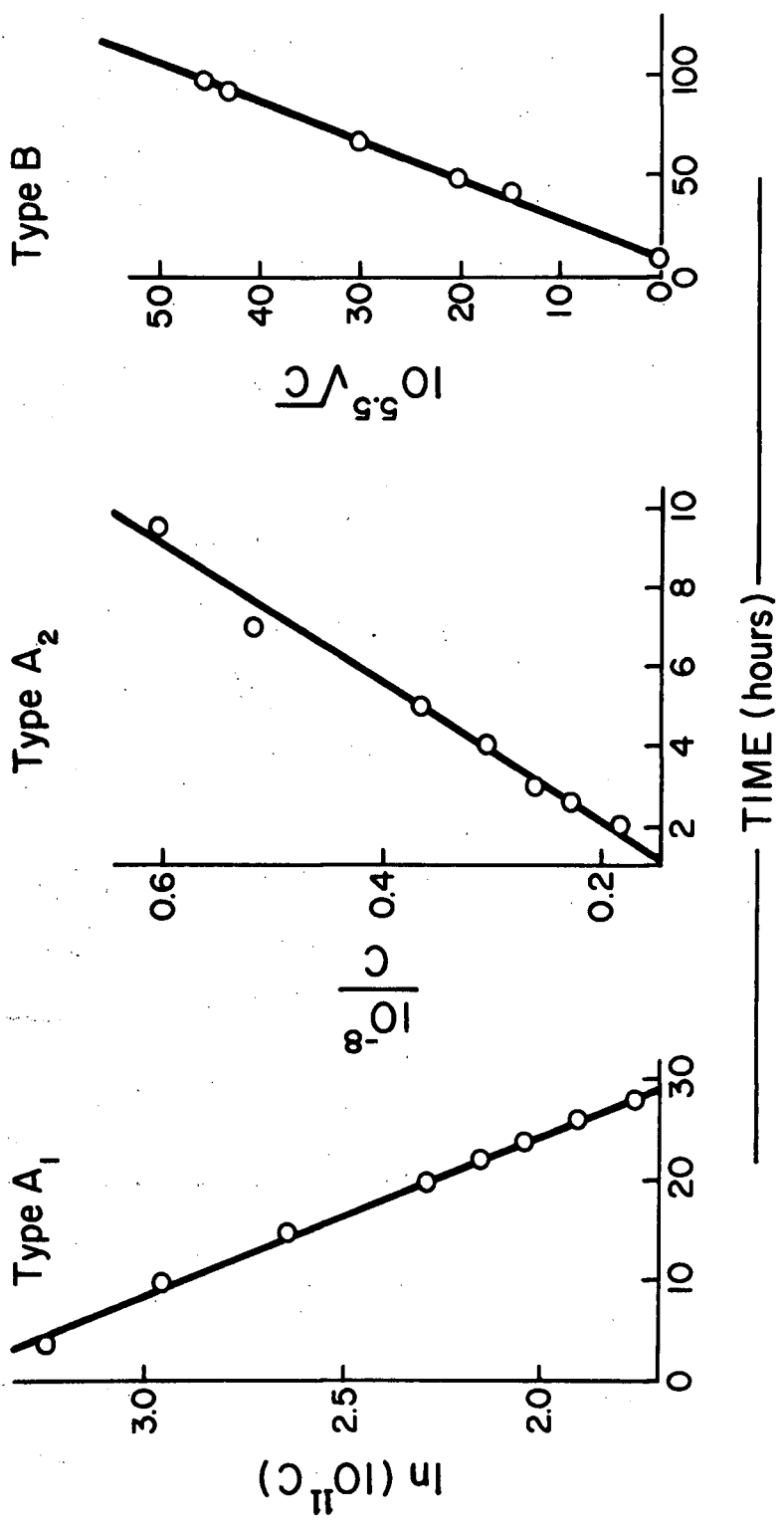
Type of Particle	C_0 ohm ⁻¹ cm. ⁻¹	Type of Behaviour
Small	1.32×10^{-12}	Type B: Nucleation; Polarization falling
Small	1.98×10^{-12}	
Small, I ₂ added	6.12×10^{-12}	Type B: Nucleation, Polarization falling
Small, I ₂ added	8.94×10^{-11}	
Large	3.26×10^{-11}	Type A ₁ : First-order Decay; Polarization constant
Large	6.24×10^{-11}	
Small	8.31×10^{-10}	
Large	1.02×10^{-9}	
Small	1.73×10^{-9}	Type A ₂ : Second-order Decay; Polarization constant
Small	1.10×10^{-7}	

slow decay of the conductance back to a value (C_∞) close to its original value (C_0). The kinetics of the decay may be first-order, type A₁ (see Figure 17), or second-order, type A₂ (see Figure 17), the latter being observed only in pellets of unusually high conductivity (Table 5). The transition from A₁ to A₂ is at about 10^{-8} ohm⁻¹ cm.⁻¹ (see Table 5). Type A₁ is undoubtedly the most commonly observed behaviour. In this type of reaction polarization remained constant or rose slightly in the course of the reaction (see Figure 16 and Table 12 in the Appendix).

FIGURE 17 - PLOTS TO TEST SHAPE OF CONDUCTIVITY-TIME CURVES:

TYPE A₁, FIRST-ORDER DECAY; TYPE A₂, SECOND-ORDER DECAY;

TYPE B, PARABOLIC RISE IN CONDUCTIVITY



(iii) The Initial Increase in Conductivity

The initial rise in conductance preceding the phenomena discussed above is difficult to handle quantitatively, since the extent to which the rise and subsequent decay are inter-related is, a priori, unknown. Also in many cases the initial rise was too rapid for accurate measurements (polarization effects limit the speed of measurement). In one type B reaction the initial rise was clearly separated from all subsequent processes and gave a good first-order plot (see Table 7 in the Appendix). In one type A₁ reaction, a first-order plot was obtained (see Figure 18 and Table 13 in the Appendix) by assuming the rise and decay are both first-order and related to each other by the equation

$$\frac{dc}{dt} = k_1 C_\infty \exp(-k_1 t) - k_2 C \quad (5)$$

On this assumption, a plot to test whether the initial reaction is first-order may be made using a quantity C' which is effectively C corrected for the occurrence of the decay. The necessary equations are derived as follows. The solution of equation (5) for C = 0 at t = 0 is

$$C = \frac{k_1 C_\infty}{k_2 - k_1} (e^{-k_1 t} - e^{-k_2 t})$$

or

$$C e^{k_2 t} = \frac{k_1 C_\infty}{k_2 - k_1} (e^{(k_2 - k_1)t} - 1)$$

If we now write

$$C' = C e^{k_2 t} \text{ and } C'_{\infty} = k_1 C_{\infty} / (k_1 - k_2)$$

we have

$$C'_{\infty} - C' = C'_{\infty} e^{(k_2 - k_1)t}$$

Taking logarithms,

$$\ln \frac{C'_{\infty} - C'}{C'_{\infty}} = - (k_1 - k_2)t$$

To find C'_{∞} when k_1 is not known, I have sometimes assumed that $k_1 \gg k_2$, so that $C'_{\infty} = C_{\infty}$; for the reaction plotted in Figure 18, C'_{∞} was found by extrapolating the decay curve back to $t = 0$. The first-order plot for the initial reaction is linear up to 5 hr., and the value of C'_{∞} is self-consistent (see Table 13 in the Appendix). Beyond 5 hr., the initial rise seems to be proceeding rather faster than equation (5) predicts. In most other experiments I have assumed that the rise is first-order, and have obtained k_1 (see Table 7 in the Appendix) from the initial slope ($k_1 C_{\infty}$) and the points t_{\max} and C_{\max} (from the curves) using equations derived from equation (5):

$$k_1 C_{\infty} e^{-k_1 t_{\max}} = k_2 C_{\max}^n$$

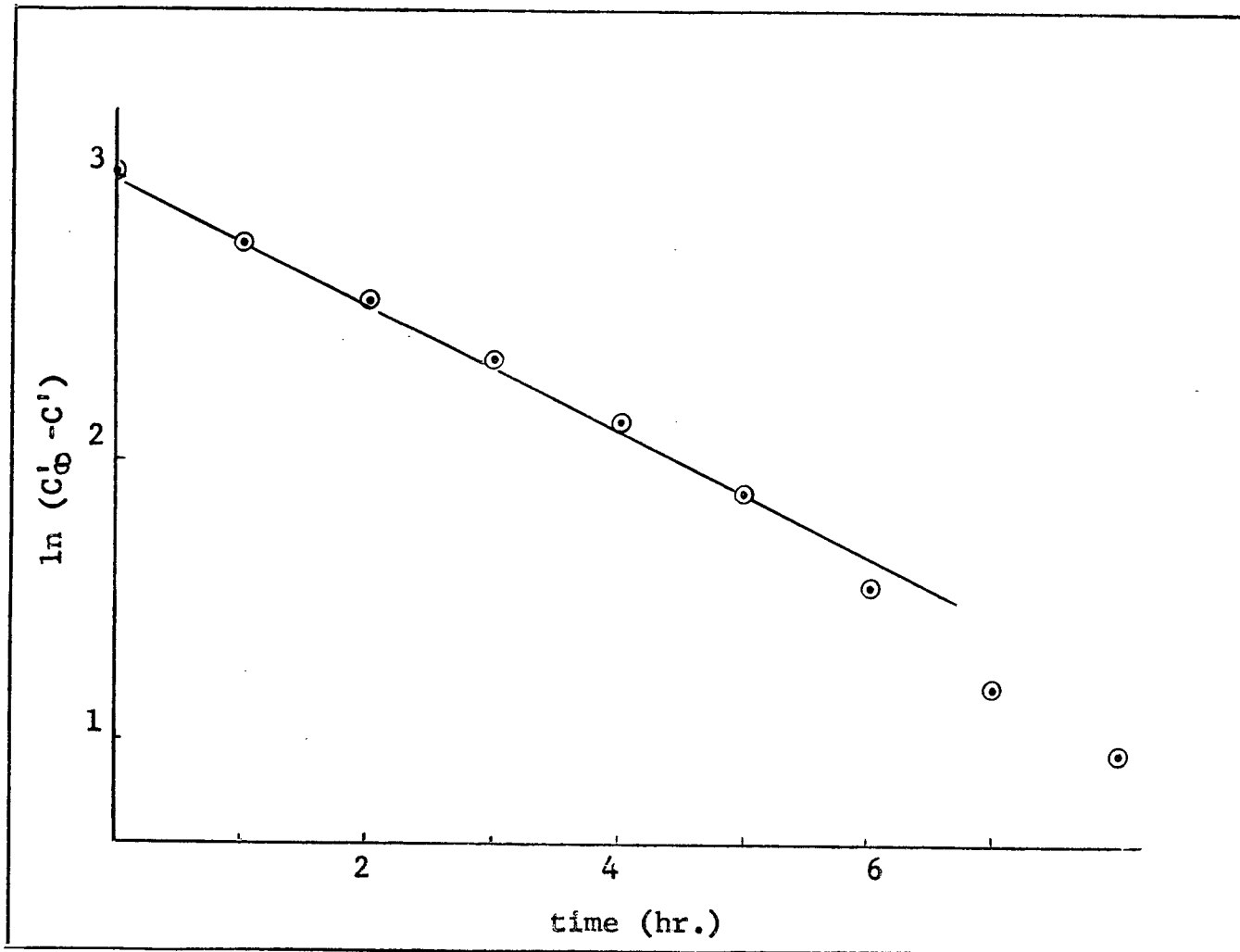
Taking logarithms, we get

$$\ln (k_1 C_{\infty}) - k_1 t_{\max} = n \ln (k_2 C_{\max})$$

or

$$k_1 = \frac{1}{t_{\max}} \ln \frac{k_1 C_{\infty}}{k_2 C_{\max}^n} \quad (6)$$

FIGURE 18 - FIRST-ORDER PLOT, TYPE A₁ REACTION (SEE TABLE 13 IN APPENDIX)



where $n = 1$ for first-order and 2 for second-order.

Sample calculation for k_1 for type A_1 reaction (see Figure 17):

$$t_{\max} = 2.2 \text{ hr.}$$

$$C_{\max} = 2.1 \times 10^{-11} \text{ ohm}^{-1} \text{ cm.}^{-1} \quad \text{from the initial curve}$$

$$k_1 C_{\infty} = 4.02 \times 10^{-11} \text{ ohm}^{-1} \text{ cm.}^{-1} \text{ hr.}^{-1} \quad \text{(from the initial slope)}$$

$$k_2 = 6.24 \times 10^{-2} \text{ hr.}^{-1} \quad \text{(from the first-order plot)}$$

Putting $n = 1$ in equation (6), and substituting the values given above, we get

$$\begin{aligned} k_1 &= \frac{1}{t_{\max}} \ln \frac{k_1 C_{\infty}}{k_2 C_{\max}} \\ &= \frac{1}{2.2} \ln \frac{4.02 \times 10^{-11}}{6.24 \times 10^{-2} \times 2.1 \times 10^{-11}} \\ &= 1.55 \text{ hr.}^{-1} \end{aligned}$$

$$k_1 = 1.55 \text{ hr.}^{-1}$$

Sample calculation for k_1 for type A_2 reaction (see Figure 17):

$$t_{\max} = 2 \text{ hr.}$$

$$C_{\max} = 5.41 \times 10^{-8} \text{ ohm}^{-1} \text{ cm.}^{-1} \quad \text{from the initial curve}$$

$$k_1 C_{\infty} = 6.61 \times 10^{-8} \text{ ohm}^{-1} \text{ cm.}^{-1} \text{ hr.}^{-1} \quad \text{(from the initial slope)}$$

$$k_2 = 5.56 \times 10^6 \text{ ohm cm. hr.}^{-1} \quad \text{(from the second-order plot)}$$

Putting $n = 2$ in equation (6), and substituting the values given above, we get

$$\begin{aligned}
 k_1 &= \frac{1}{t_{\max}} \ln \frac{k_1 C_{\infty}}{k_2 C_{\max}^2} \\
 &= \frac{1}{2} \ln \frac{6.61 \times 10^{-8}}{5.56 \times 10^6 \times (5.41)^2 \times 10^{-16}} \\
 &= 0.673 \text{ hr.}^{-1} \\
 k_1 &= 0.673 \text{ hr.}^{-1}
 \end{aligned}$$

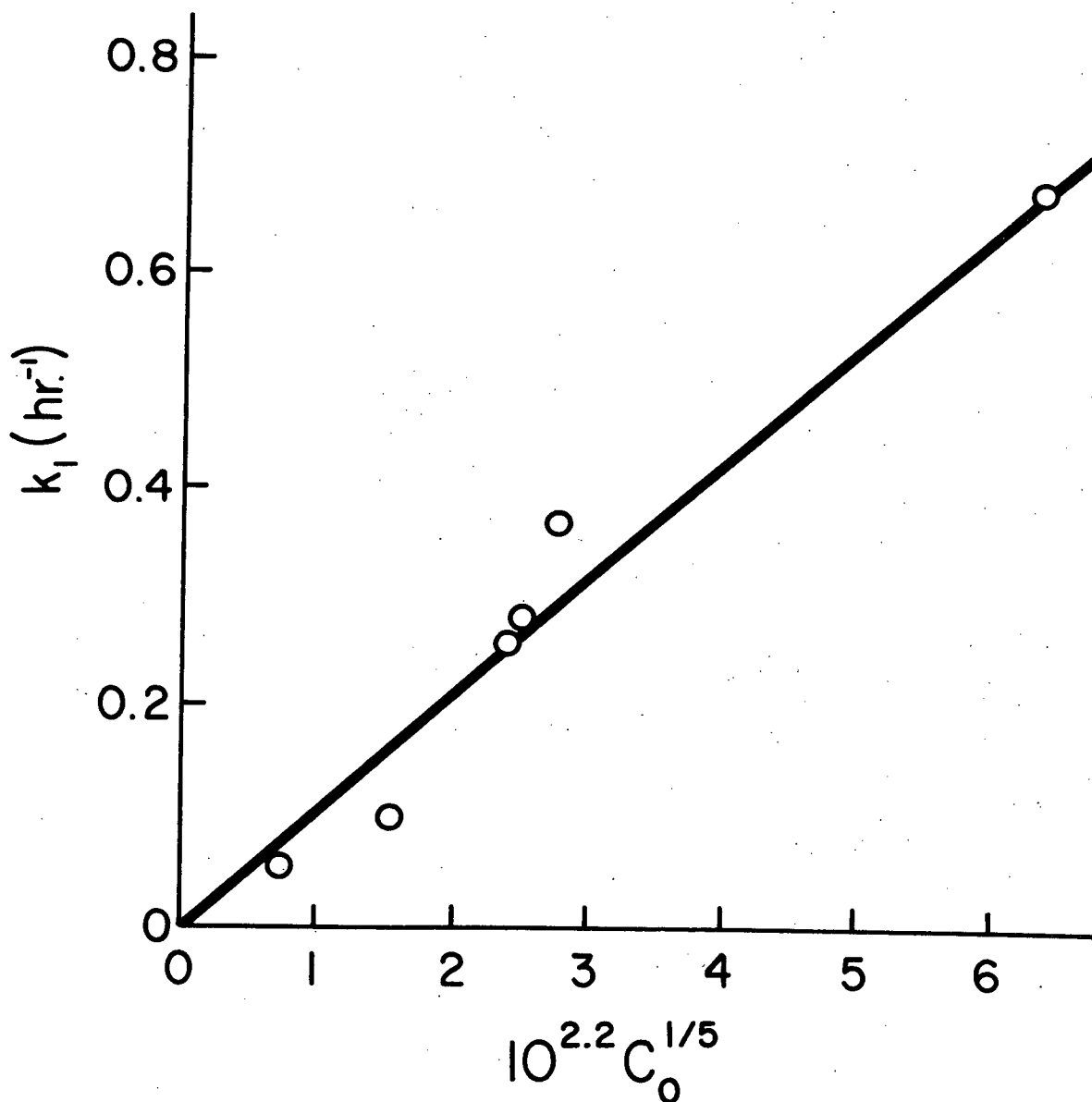
k_1 shows no correlation with Chlorine pressure (in the range 13-54 cm. Hg - see Table 7 in Appendix), but shows a slow monotonic increase with C_0 , which seems to be best represented by $k_1 \propto C_0^{1/5}$ (see Figure 19).

(iv) Type B Reactions

As indicated previously type B behaviour is a second rise in conductivity accelerating in a manner characteristic of reactions involving a new solid phase (Fig. 16). In the KI/Cl₂ system, this behaviour was found only rarely, for pellets of exceptionally low conductivity (see Table 5). However, when this type of behaviour occurred, the rise in conductivity continued for a very long time (about 100 hr.) and very precisely followed the square of the time (see Figure 17). Type B behaviour has not been observed in a pure KI pellet with initial conductivity greater than $10^{-12} \text{ ohm}^{-1} \text{ cm.}^{-1}$ (see Table 5), but addition of Iodine during precipitation of small particles appears to increase this limit to $10^{-10} \text{ ohm}^{-1} \text{ cm.}^{-1}$

FIGURE 19

CORRELATION OF RATE CONSTANT FOR INITIAL RISE
WITH INITIAL CONDUCTIVITY OF PELLET



(see Table 5). In both examples of this type of reaction, the accelerating regions are of much shorter duration than in pure pellets of very low C_0 , and neither gave a good parabolic plot. In one of them, a good plot was obtained for $C \propto t^{2.5}$, 0 to 3 hr.

For the KI/F₂ system, by contrast, a type B curve was obtained in nearly every reaction (Fig. 20). The accelerating portion could not be represented by a single power of the time, but it was usually either parabolic (Fig. 21) or cubic initially, with rather erratic behaviour later (see Figure 26 and Table 11 in the Appendix).

The polarization behaviour in type B reactions was quite different from type A. In all KI/F₂ reactions and in KI/Cl₂ reactions with pure KI, the polarization decreased markedly in the course of the reaction, suggesting that the conductivity was becoming electronic. (In one of the KI/Cl₂ reactions, the polarization at first increased, but then decreased steadily; in the other, it decreased rapidly and actually vanished after about 70 hr.; runs S VI and S I, see Table 12 and Figure 16). The reactions with F₂ being faster than those with Cl₂, it was feasible to prolong the experiments further into the period of falling conductivity at the end of the reaction and to show that the polarization increased in this period (see Figure 20 and Table 12 in the

FIGURE 20
REACTION OF PRESSED PELLET WITH F_2 ;
CONDUCTIVITY AND POLARIZATION CURVES

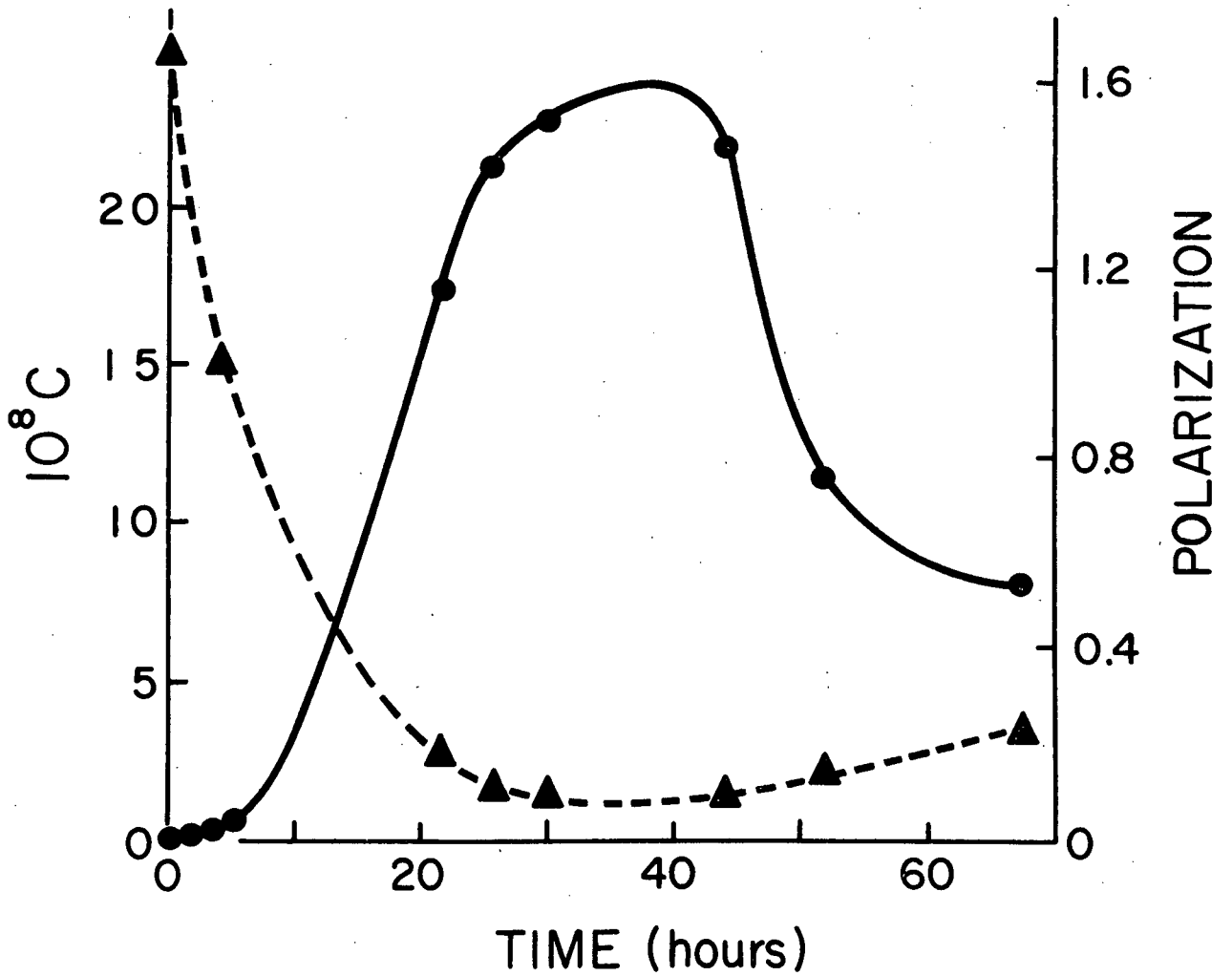
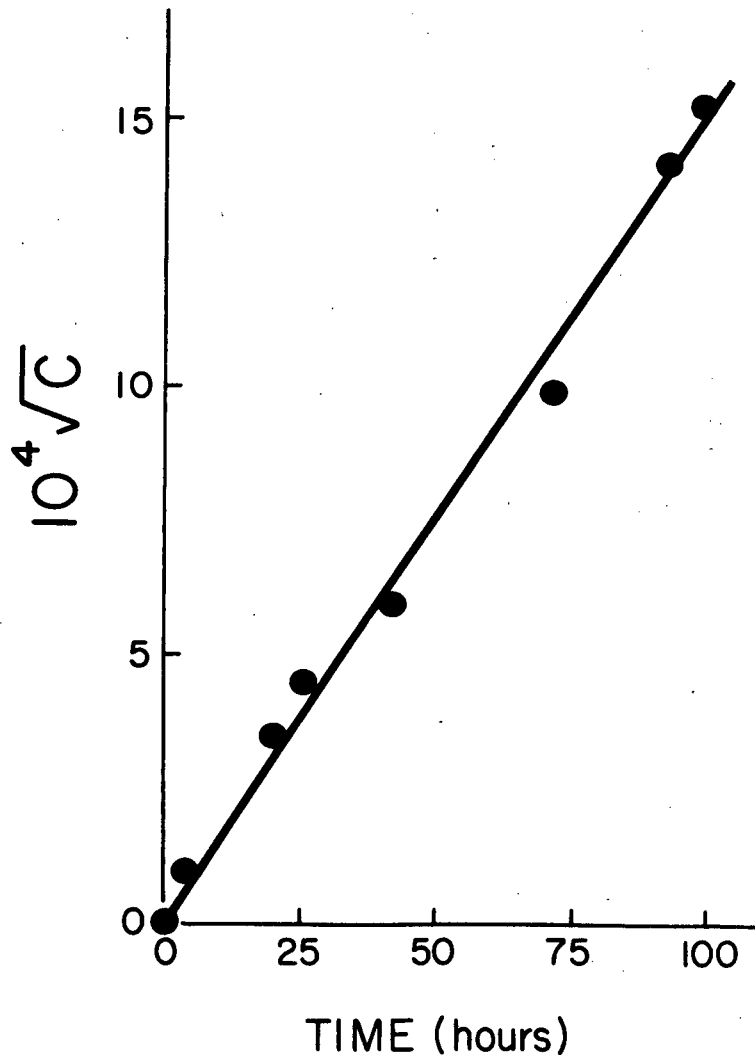


FIGURE 21.

TYPE B, PARABOLIC RISE IN CONDUCTIVITY (KI/F₂ SYSTEM)

Appendix), as expected if the system is reverting to ionic conductivity.

(v) The Appearance of the Reacted Pellets

The appearance of the pellets on breaking them after reaction differs according to the type of the behaviour.

Type A: The pellet is coloured uniformly light brown throughout, while its surface may show black and white markings.

Type B: In one KI/Cl₂ reaction, a completely blackened zone extended inward from all faces of the pellet to a depth of 0.2 to 0.5 mm., and was sharply separated from the white interior of the pellet. In the other, the regions were reversed, a black central region being surrounded by a light brown border. For the KI/F₂ reactions, there was frequently very little colour developed (Appendix, Tables 7 and 11).

D. Changes of Electrical Conductivity during the Reaction of Other Types of KI Sample with Cl₂(g)

(i) Single Crystal

Preliminary results of a spectrophotometric study of the oxidation of single crystals of KI in this laboratory (45) have indicated the formation of Iodine (absorbing in the visible) and V-Centres absorbing at 3600 Å and 2800 Å. The reaction terminates within 17 hours and corresponds to oxidation

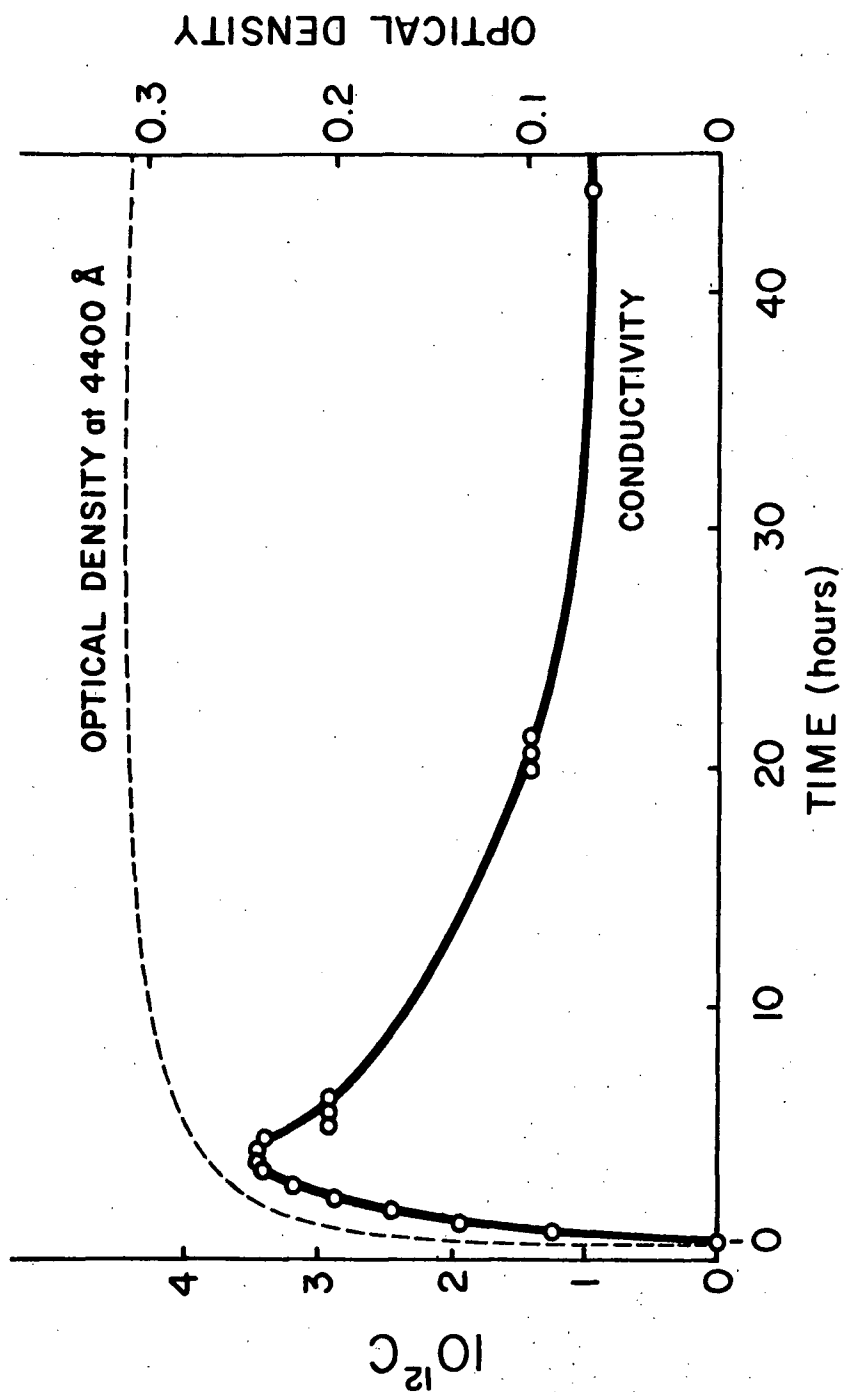
of a zone a few thousand Å⁰ thick or about 0.1% of the crystal. This is the only type of material in which the kinetics and conductivity changes have been compared directly. (The changes in the conductivity were at the limit of detection of the electrometer.) The most significant feature of the results is that the amount of Iodine is increasing slowly during most of the type A (A₁) decay of the conductivity (see Figure 22).

(ii) Powder

Measurement of the electrical conductivity during the reaction showed no detectable change in times up to 28 hours, for a bed of powder about 3 mm. thick and 12 mm. in diameter, having a conductance at room temperature of about 10^{-11} ohm⁻¹ cm.⁻¹. (The resistance of the connecting leads was 10^{13} ohm cm.)

FIGURE 22

REACTION OF SINGLE CRYSTAL WITH Cl_2 ; COMPARISON OF CONDUCTIVITY
CHANGES AND KINETICS OF IODINE FORMATION



DISCUSSION

In discussing electronic defects, I shall use Harrison's notation (35), where a and c represent anion and cation sites, and ion signs for structures within the solid represent effective charges. Thus a^+ and c^- are vacant sites, $I(a)^+$ is a positive hole, and, e.g., $I(a)_2^{++}(c_2)^{--}$ is a pair of holes trapped by two cation vacancies. Such formulae will be used below to show the number of holes and vacancies in any trapped hole-centre postulated. I have no new evidence relevant to the covalent bonding in such centres. For example, any argument in which I use a dissolved I_2 molecule, $I(a)_2^{++}(c_2)^{--}$, would be unaffected if I wrote it as a dissolved I_3^- ion, $I(a)_3^{++}(c_2)^{--}$.

A. Ionic Conductivity of KI as a Function of Temperature

The ionic conductivity of a number of alkali halides above 250° C. has been studied extensively by a number of workers, but very little work has been done on the conductivity of alkali halides below 250° C. Dreyfus and Nowick (28) have studied the conductivity of NaCl from above 400° C. down to -35° C.

It was the purpose of this study to determine the conductivity of KI from 330° C. to 22° C. (room temperature) and thus (a) to throw some light on the behaviour of defects

at low temperatures and (b) to overlap the structure sensitive region for KI, as previously reported by Lehfeldt (50), and thus compare the activation energy and the absolute value of conductivity in this region with those obtained by Lehfeldt. The study of the conductivity of KI as a function of temperature has shown behaviour quite different from that of NaCl single crystals.

The conductivity plot ($\log C$ vs. $1/T^\circ K.$) made for KI in the temperature range $22^\circ C. - 330^\circ C.$, divides itself into 2 distinct regions (DE and EF) (see Figure 15). Region EF (same figure) overlaps with the structure sensitive region for KI, as previously reported by Lehfeldt. The activation energy for the motion of cation vacancies calculated in this region is in good agreement with that obtained from a similar region of Lehfeldt's plot. However, the absolute value of conductivity at $300^\circ C.$ as obtained from my results ($3.18 \times 10^{-7} \text{ ohm}^{-1} \text{ cm.}^{-1}$) is greater by a factor of 30 when compared to Lehfeldt's result (50) for the same temperature. This discrepancy in the value of conductivity is most probably attributable to the purity of KI samples, since it seems very likely that the temperature range in which $E_{\infty} = 0.82 \text{ eV.}$ is an impurity region analogous to the well-investigated impurity region of NaCl. Region DE represents behaviour unlike any

previously observed in an alkali halide. There appears to be a sharp decrease in activation energy below 92° C. (Region DE). The activation energy in this region is actually less than the activation energy for the migration of cation vacancies in the bulk. The activation energy for the migration of cation vacancies in the bulk for KI can be obtained from the structure sensitive region (or impurity region). This value as reported before is 0.817 eV. according to our results (and 0.822 eV. according to Lehfeldt). Now in any region below the structure sensitive region, the observed activation energy would normally be expected to be greater than that in the structure sensitive region. At all temperatures below the structure sensitive region the activation energy should be composed of two terms, one associated with the mobility of cation vacancies, and the second arising from the association of vacancies with impurities or from the heat of solution of impurities.

Dreyfus and Nowick have found high activation energies (as expected) (28) for the migration of cation vacancies below the structure sensitive region for cation-doped NaCl, and have been able to interpret their results precisely in terms of the multivalent cationic impurities present in the system. My results for KI are in complete contrast with Dreyfus and Nowick's results for NaCl, and can not be interpreted in terms of

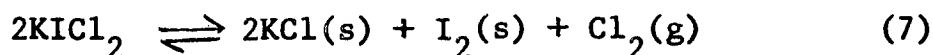
multivalent cationic impurities present in the system. To account for the almost negligible activation energy observed in Region DE of our plot, it is suggested that either (1) vacancies are in a region of unusually high mobility, such as dislocations, or (2) vacancy concentration is increasing with falling temperature. This may arise from the space-charge effect, which amounts to an adsorption of anion vacancies at dislocations and consequent increase of cation vacancy concentration in the surrounding region. This effect, like most adsorptions, is expected to be most important at low temperatures and could give a negative contribution to the activation energy.

Both explanations attribute the effect to dislocations. It is therefore suggested that the vacancy concentration at low temperatures is completely controlled by dislocations, rather than by impurities. On this basis, the dependence of the initial conductivity C_0 of a pellet on the conditions of preparation is fairly readily explained. It was found (see Table 2 in Results) that rigorous drying of the powder led to generally high conductivities. It seems probable that the effect of rigorous drying is to prevent the grain boundary structure from being lost by recrystallization after pressing. In material which is "wet" during

pressing, the grain boundaries can be largely destroyed by subsequent recrystallization, with a consequent decrease in the associated space-charge of cation vacancies and in C_0 .

B. The Nature of the Products (KI/Cl₂ Reaction)

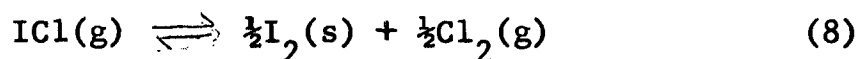
The nature of the new ionic solid produced is of some significance in relation to the mechanism of reduction of Chlorine at the KI surface. Polyhalides should be stable, relative to KCl and I₂, at Chlorine pressures exceeding the equilibrium constant K for the reaction



K may be calculated from the following known thermodynamic data (53):

(a) the dissociation pressure of KICl_2 into KCl and ICl, which is $K_1 = p_{\text{ICl}} = 9.3 \text{ mm. Hg}$ at 25° C. ;

(b) the equilibrium constant K_2 for



for which (54) $\Delta F^\circ = 977 \text{ cal. (thermochemical)}$ or 5751 cal.

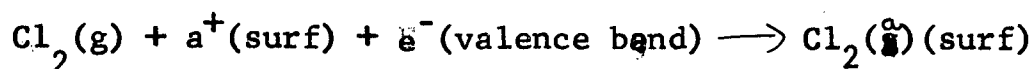
(spectroscopic). From these data, $K_2 = 5.2 \text{ atm.}^{-\frac{1}{2}}$ or $3.6 \text{ atm.}^{-\frac{1}{2}}$.

KICl_2 should thus be stable at 25° C. at any Chlorine pressure above $p_{\text{Cl}_2} = K = K_1^2 K_2^2 = 3.1$ or 1.5 mm. Hg. Yet the principal products are KCl and I₂ in our experiments at 512 mm. Hg.

It is therefore concluded that the Cl_2 molecules which attack the surface cannot reorganize to form ICl_2^- ions (with I as the central atom). This seems very reasonable from the steric considerations illustrated in Figure 23.

(1) An isolated ICl_2^- ion is a complete misfit in the KI lattice. It is too large to occupy a single anion vacancy, and much too small to span three anion sites. The distance between the adjacent I^- ions (4.99 \AA) exceeds the entire Cl-I-Cl distance in the polyhalide ion (4.68 \AA).

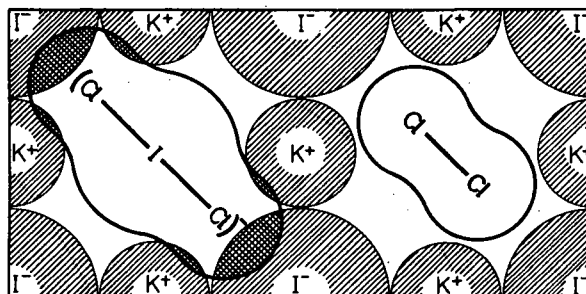
(2) A Cl_2 molecule will fit easily into a single anion vacancy, where it can probably pick up an electron to form a molecule-ion (Cl_2^-) and migrate in the surface to a growing KCl crystal before the Cl-Cl bond is broken. (I wish to thank Dr. N. Bartlett for pointing out that the Cl_2^- molecule ion is probably not much bigger than the Cl_2 molecule, since the extra orbital will not be pure antibonding $\sigma^* 3p$. Both this orbital and some already occupied in Cl_2 must have considerable d-character, to account for the dissociation energy of Cl_2 being greater than that of F_2 .) Thus the probable reactions at the surface may be written



These two equations suggest that the initial rate of reaction

FIGURE 23

FIT OF Cl_2 MOLECULE AND MISFIT OF ICl_2^-
IN AN ANION VACANCY IN KI



is proportional to the concentration of anion vacancies in the surface. However, the initial rate of oxidation of KI powders was found to be correlated with C_0 (see Figure 19), which represents the cation vacancy concentration in the bulk. This can be explained in terms of the space-charge effect which leads to a correlation between the anion vacancies in the surface and the cation vacancies in the bulk.

The initial step is first-order because the abstraction of electrons from the valence band is counterbalanced by flow of cation vacancies into crystal (see below), and the increase of cation vacancy concentration in the bulk will be first-order if the first step is rate controlling.

No similar product analysis has yet been made for the KI/F₂ reaction, in which the formation of polyhalides is, a priori, more probable than KI/Cl₂.

Reaction Steps in the Bulk, Involving Holes and Vacancies

The KI/Cl₂ and KI/F₂ reactions may now be discussed together. For the KI/Cl₂ reaction, it is necessary to explain the occurrence of the two types of behaviour designated "type A" and "type B" in the Results section above. For the KI/F₂ system, type B reactions only were observed. I shall therefore discuss principally the KI/Cl₂ reaction; and what is said about the type B mechanism is equally applicable to KI/F₂.

It is supposed that the oxidation at the surface produces positive holes in the valence band and demands a supply of cations. These probably migrate most easily close to the grain boundaries, and two equal and opposite electric currents are established from the surface into the pellet: positive holes moving directly into the bulk and cation vacancies moving near to the grain boundaries and thence into the bulk. The observed changes in the electrical conductivity during reaction must be explained in terms of the formation of these holes and vacancies, and the ways in which they may combine. In these terms the existence of the two distinct categories of reaction (A and B) may be explained in terms of different trapping processes for positive holes, as follows:

- (a) If the initial cation vacancy concentration is high (as indicated by high conductivity) most of the positive holes will be trapped at isolated cation vacancies in the bulk (see Figure 24); this is identified with type A behaviour.
- (b) If the initial vacancy concentration is low, trapping will take place close to grain boundaries, as new cation vacancies emerge from them. This situation favours the formation of clusters of positive holes and hence nucleation of solid Iodine at the grain boundaries (see Figure 25); this is

FIGURE 24

PROPOSED MECHANISM OF A TYPE "A" REACTION

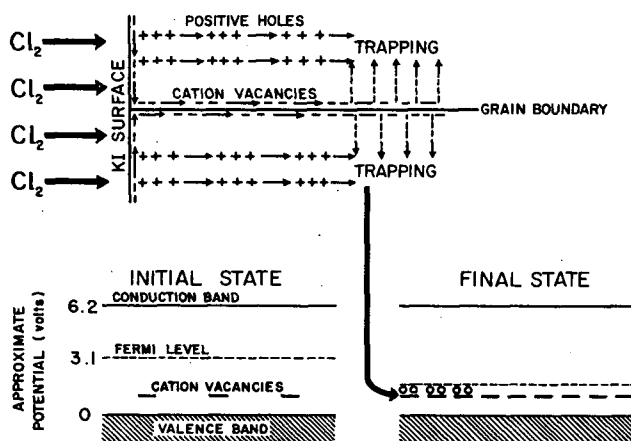
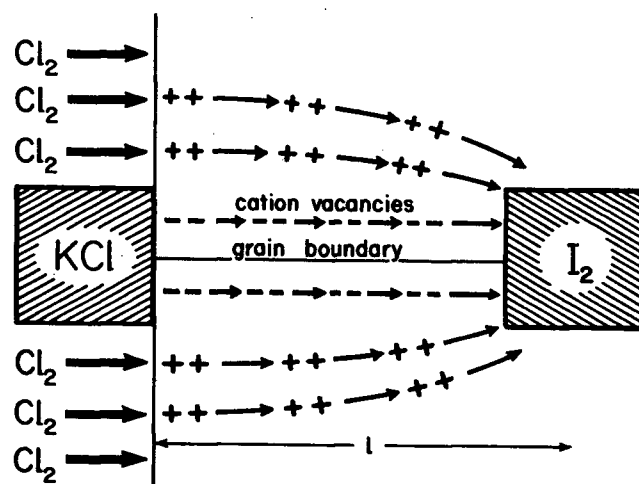


FIGURE 25

PROPOSED MECHANISM OF A TYPE "B" REACTION



identified with type B behaviour.

Type A Behaviour

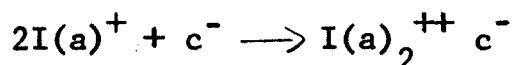
This type of behaviour is found for high initial cation vacancy concentrations (high conductivity, a condition favouring the trapping of positive holes at isolated cation vacancies - see Figure 24). If the holes are trapped in the ratio of one hole to each new cation vacancy created, then the system of defects constitutes an impurity level (in the terminology of band theory) which at large extents of reaction is half-occupied and thus coincides with the Fermi level (E_f). Since E_f is initially about 3 eV. above the valence band (taking band gap (55) as 6.2 eV.) and the defect level (E_v) is probably no more than 1 V. above the same datum, the drop in the Fermi level is of the order of 2 V. (see Figure 24). Most of this drop occurs in the early stages of reaction. If N_h and N_v are total numbers of positive holes and cation vacancies at any time, the Fermi-Dirac distribution law leads to

$$E_f - E_v = KT \ln \frac{2N_v - N_h}{N_h} \quad (9)$$

If the vacancies formed in the reaction are only equal in number to those initially present, $N_v = 2N_h$ and E_f is already only 0.03 V. above the defect level. Thus the KI rapidly

becomes less oxidizable, and the reaction proceeds only to a very small extent.

This mechanism thus readily explains why the pellet ceases to be oxidizable by Chlorine after only a very small amount of reaction. It remains to explain why the conductivity rises in the early stages of the reaction, at the same time apparently remaining ionic, as indicated by the observation that polarization effects do not decrease during the rise in conductivity. This suggests that, in the course of the trapping processes, some lattice vacancies are left in excess. Such a conclusion is contrary to the earlier ideas of trapping processes (Seitz) in which it was considered that trapped-hole centres would most usually be electrically neutral. Seitz proposed one structure (V_3) containing one hole trapped at two vacancies; but in the present work, it is necessary to postulate that two holes are trapped at one vacancy, in order to leave vacancies in excess,



Such a trapping process is not unreasonable if the formation of a covalent bond between the two I atoms is taken into account, as well as the electrostatic attraction of the holes to the vacancy. If this is the trapping process, equation (9) may

be rewritten as

$$E_f - E_v = KT \ln (1 + C_o / C) \quad (10)$$

Thus C_o / C_∞ should have the same value in all experiments, corresponding to $(E_f)_\infty$, the chemical potential of reduced Cl_2 at the surface. Table 15 (Appendix) shows that, for pressed pellets, C_o / C_∞ varies within a factor of about 9; but this represents a range of only 0.016 V. in $(E_f)_\infty - (E_v)$, and is attributable to minor structural changes in the surface or bulk. Table 15 (Appendix) suggests a systematic difference between large and small particles, but this is not well established. For type B behaviour, C_∞ / C_o has strikingly different values, and is not to be interpreted in the same way. (In these cases, C_∞ still represents the end of the initial reaction, before the parabolic rise.)

Types A_1 and A_2 Decay

A_1 Decay

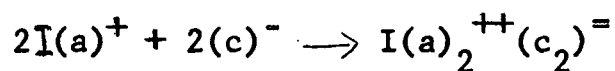
First order (A_1) decay of the ionic conductance requires the vacancies to be destroyed at trapping sites present in great excess. This has been pointed out by Dreyfus and Nowick (28) in a recent study of the decay, below room temperature, of a frozen-in excess of cation vacancies in NaCl. They found first-order kinetics, but did not attempt to identify the trapping sites responsible. It is probable

that A_1 decay represents a recombination of vacancies with the grain boundaries or dislocations. This may be assisted by oxidation at the surface, which should enhance the flow of anion vacancies into the bulk to counterbalance the change of the cation vacancies. The continued slow production of Iodine during oxidation of a single crystal (see Figure 22) supports this view.

A_2 Decay

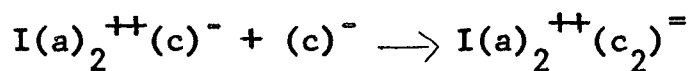
Second-order decay (A_2) is much less common and occurs only for pellets with an unusually high initial conductance. This observation is consistent with any explanation in which two defects present in equal concentration combine with each other; such a process may be expected to become important only at much higher defect concentrations than those at which the principal process is the absorption of the defect at centres present in excess. There are two obvious possibilities:

(1) Two positive holes may be trapped by two cation vacancies (in a second-order trapping process independent of the first, and slower than it, so that it becomes noticeable only in the later stages of the reaction),



(2) The combination of the defect $\text{I}(\text{a})^{++}(\text{c})^-$ with another cation vacancy; the two reacting species are present in

roughly equal concentration,



Type B Behaviour

By analogy with the kinetics of many solid phase decompositions, it seems most likely that the sigmoid rate curves of type B behaviour are to be explained in terms of the formation and growth of nuclei of the reaction products. If we consider first the growth of a single I_2 nucleus below the surface of the KI, connected by a grain boundary to a growing KCl crystal on the surface (see Figure 25), we may arrive at one possible explanation of the parabolic portion of the rate curve (see Figure 17) as follows: The surfaces of the growing I_2 nuclei will act as trapping sites for positive holes. Since a process which increases the surface area, such as the formation of a kink in a step on the receding KI surface, also forms a trapping site, the number of trapping sites is proportional to the surface area of the growing nuclei. In consequence, the equal and opposite hole and vacancy currents (see Figure 25) should be proportional to the surface of the nuclei. This leads at once to a growth law in which each nucleus has a constant linear rate of growth, the number of charge carriers is proportional to the square

of the time (observed parabolic law for conductance) and the amount of product is proportional to t^3 . Suppose that a cubical nucleus of side x at time t is situated at a depth l below the surface of the pellet. The E.M.F. of the positive hole transfer cell is E [$\text{Cl}_2(\text{g})/\text{KCl} \mid \text{KI}/\text{I}_2(\text{s})$, standard E.M.F. 0.89 V.], and the overall mobility of the charge carriers is U ($U^{-1} = U_v^{-1} + U_h^{-1}$, where U_v and U_h refer to vacancies and holes). The current is related to the number and mobility of charge carriers and the E.M.F. of the cell by

$$i = neEU/l^2 \quad (11)$$

(where i is the current due to holes or vacancies, n is the number of charge carriers (holes or vacancies) and e is the electronic charge). If a charge carrier is produced for every ion-pair in the surface of the nucleus, and the nearest neighbour distance in KI is a (3.53 Å), then

$$n = 3x^2/a^2 \quad (12)$$

(where x , V = cube side and volume of a nucleus). The current is therefore

$$i = 3x^2 eEU/a^2 l^2 \quad (13)$$

The rate of growth of a nucleus

$$\frac{dV}{dt} = 3x^2 \frac{dx}{dt} = V_m i/F \quad (14)$$

is proportional to the current i (V_m is the molar volume of KI)

and F is the Faraday). Combining equations (11), (12) and (14) and integrating with $x = 0$ at $t = t_0$, we get

$$\begin{aligned} x &= K(t-t_0) \\ n &= 3(K^2/a^2)(t-t_0)^2 \\ V &= K^3(t-t_0)^3, \text{ where } K = \frac{V_m eEU}{a^2 l^2 F} \end{aligned} \quad (15)$$

Since the conductivity of a pellet is proportional to n , equation (15) explains the parabolic curve (see Figure 17). This mechanism is in qualitative agreement with the following evidence available from the simultaneous study of the KBr/Cl_2 system by Catton in this laboratory:

- (1) The microscopic observation of Br_2 -filled cavities (about 30μ below the surface) in reacted KBr crystals (see Figure 3). This observation agrees very well with the mechanism proposed for the KI/Cl_2 reaction as illustrated in Figure 25. (Unfortunately the observation of halogen-filled cavities could not be carried out on the reacted single crystal of KI , because no single crystal of KI has been found to give a type B reaction.)
- (2) The mechanism for the KBr/Cl_2 reaction has been postulated in terms of growing KCl layer overtaking the layer of cavities and absorbing the Br_2 , followed by formation of a new layer of cavities. This would explain why the reacted KI pellets, like the reacted KBr single crystals, had an outer-reacted zone sharply separated from an unreacted centre.

Such an explanation would fit the observations for KI, but it removes the simple explanation of parabolic law since the distance l between the KCl/KI interface and the halogen nuclei becomes time-dependent; the laws observed by Morrison for KBr/Cl₂, involve much higher powers of time, and are more consistent with the mechanism. However, there is probably considerable error in applying a treatment for a single nucleus to a system containing many nuclei with overlapping conduction paths, and this overlap is probably more significant in the KI pellets than in the KBr single crystals, wherein the Br₂ nuclei could be seen microscopically to be quite widely separated.

Factors Determining the Type of Reaction

Type A reactions occur when the initial cation vacancy concentration in the bulk is high. At low vacancy concentrations, trapping will take place close to the grain boundaries, as new vacancies emerge from them. This situation favours the formation of clusters of trapped holes, leading to nucleation and type B behaviour. (Type B behaviour in the KI/F₂ system may be explained in terms of (a) low C_0 of the KI pellets, (b) F₂, being a much more drastic oxidant than Cl₂, is more efficient in abstracting electrons from the anion band of KI, and thus creates excess positive holes.) In pellets with

added I_2 , the conductivity and polarization effects indicated the type A and type B trapping processes were occurring simultaneously. The type B rise in conductivity started early, because I_2 nuclei were present right from the beginning, and finished early, as the number of bulk trapping sites rises. Even when the bulk Fermi level has fallen to that of the oxidant, the system of vacancies can still form an effective barrier, kinetically, to the passage of positive holes. (The situation is analogous to the passage of gas molecules through a capillary on the wall of which they can be adsorbed reversibly.) In the oxidation of KBr (43), type B behaviour is the rule rather than the exception. In this less oxidizable material, the bulk Fermi level has not so far to fall before type A reaction ceases, and the cation vacancies cannot build up in sufficient numbers to prevent holes from reaching the grain boundaries.

Oxidation of Unpressed Powders

The absence of any change in the conductivity indicates that oxidation of powders occurs without change in the bulk defects of each crystal. There is thus little analogy between the oxidation mechanisms of large and small crystals (which is familiar also for reduction of silver halides in the photographic process). The obvious interpretation of this

result is that the oxidant removes electrons from the bound surfaces before attacking the bulk. If the migration of the products to nuclei of KCl and I_2 is sufficiently rapid, an essentially fresh surface will always be exposed to the gas, and the KI crystals will diminish in size by stripping off successive layers without change in the underlying bulk. The rate of the reaction will be proportional to the surface area of the KI, and will be essentially constant for the first few per cent of the reaction as was found experimentally (see Figure 12).

APPENDIX

(Summary of Experimental Results)

TABLE 6

KINETIC RESULTS FOR THE KI/Cl₂ REACTION (POWDERED SAMPLE)

No. of days KI(s) exposed to Cl ₂ (g)	Moles of I ₂ (produced) per Mole of KI (used)	Average value	% KI oxidized
1	1.50x10 ⁻³		
"	3.42x10 ⁻³		
"	5.70x10 ⁻³	3.3x10 ⁻³	0.60
"	2.50x10 ⁻³		
2	6.70x10 ⁻³		
"	4.13x10 ⁻³	5.21x10 ⁻³	1.00
"	4.80x10 ⁻³		
5	19.09x10 ⁻³		
"	7.97x10 ⁻³	13.53x10 ⁻³	2.70
6	21.25x10 ⁻³		
	6.76x10 ⁻³	14.00x10 ⁻³	2.80
9	3.0x10 ⁻²		
	3.0x10 ⁻²	3.0x10 ⁻²	6.0

TABLE 7

TABULATED DATA FROM ELECTRICAL CONDUCTIVITY MEASUREMENTS IN KI/Cl₂ REACTION

(L and S represent large and small particles respectively)

Run no. and date	P _{Cl₂} (cm. Hg)	Type of KI sample	10 ¹¹ C _o ohm ⁻¹ cm. ⁻¹	Growth (k ₁ in hr. ⁻¹)	Decay (k ₂ may be first or second order)	Type B accelerating region
L II 26 Jul 1962	21	L	6.24	0.665	0.726 hr. ⁻¹ (First-order)	---
L IV 20 Aug 1962	21	L	3.26	1.550	0.0624 hr. ⁻¹ PLOT:First-order	---
L V 12 Dec 1962	21	L	8.91	NO REACTION	---	---
L VI 18 Dec 1962	21.3	L	129	0.282	1.06 hr. ⁻¹ PLOT:First-order	---
S I 15 Jan 1963	21.3	S	0.13	0.178 PLOT:First-order (no interference from decay)	---	PLOT:C ∝ t ² (0-91 hr.) (Fig. 17) Pellet had outer dark zone.
S II 12 Mar 1963	13.7	OS.	83.1	0.264 PLOT:First-order (corrected for decay, Fig. 18)	0.0148 hr. ⁻¹ PLOT:First-order	---
S III 25 Mar 1963	16.3	S	173	0.370	5.73 ohm cm.hr. ⁻¹ PLOT:Second-order	---
S IV 5 Apr 1963	22.0	S	11,000	0.673	5.55 ohm cm.hr. ⁻¹ PLOT:Second-order	---

TABLE 7 (continued)

TABULATED DATA FROM ELECTRICAL CONDUCTIVITY MEASUREMENTS IN KI/Cl₂ REACTION

Run no. and date	P _{Cl₂} (cm. Hg)	Type of KI sample	10 ¹¹ C _O ohm ⁻¹ cm. ⁻¹	Growth (k ₁ in hr. ⁻¹)	Decay (k ₂ may be first or second order)	Type B accelerating region
S V 20 Apr 1963	13.0	S (I ₂ added)	0.61	---	---	PLOT: C ∝ t ^{2.5} (0-3 hr.)
S VI 16 May 1963	54.0	S	0.19	0.056	---	PLOT: C ∝ t ² (0-120 hr.) Pellet had inner dark zone
S VIII 25 May 1963	31.0	S (I ₂ added)	8.94	0.10	---	Irregular shape (0-25 hr.)
Unnumbered 31 May 1963	26.0	single crystal	1.85	0.595	0.10 hr. ⁻¹ (First-order)	---
Unnumbered 5 Jun 1963	24.0	unpressed powder	1.33	---	---	---

TABLE 8

ELECTRICAL CONDUCTIVITY OF KI (250°-680°)C.; LEHFELDT (50)

$t^{\circ}\text{C}$	$T^{\circ}\text{K}$	$10^3/T^{\circ}\text{K}$	$\log C$
250	523	1.91	<u>9.000</u>
275	548	1.82	<u>9.446</u>
300	573	1.74	<u>9.902</u>
325	598	1.67	<u>8.000</u>
350	623	1.60	<u>8.300</u>
375	648	1.54	<u>8.778</u>
400	673	1.48	<u>7.300</u>
450	723	1.38	<u>7.698</u>
500	773	1.29	<u>6.300</u>
550	823	1.21	<u>6.778</u>
600	873	1.14	<u>5.300</u>
680	953	1.04	<u>4.000</u>

TABLE 9

ELECTRICAL CONDUCTIVITY OF KI (22°-330°)C.; THIS WORK

$t^{\circ}\text{C}$	$T^{\circ}\text{K}$	$10^3/T^{\circ}\text{K}$	$\log C$
22	295	3.38	<u>12.902</u>
53	326	3.06	<u>12.933</u>
66	339	2.94	<u>12.989</u>
94	367	2.72	<u>11.098</u>
116	389	2.56	<u>11.814</u>
159	432	2.31	<u>10.748</u>
183	456	2.18	<u>9.148</u>
234	507	1.96	<u>8.411</u>
269	542	1.84	<u>8.712</u>
330	603	1.66	<u>7.502</u>

TABLE 10
SPECIFICATION FROM MALLINCKRODT CHEMICAL WORKS
OF THE KI USED IN THIS WORK
POTASSIUM IODIDE AR (ACS) CRYSTALS - CODE 1121

Appearance and Odor	Transparent, colorless crystals. Odorless.
Insoluble Matter	0.005% max.
Sulfate (SO ₄)	0.005% max.
Loss on Drying	0.20% max.
pH of a 5% Solution (25° C.)	6.0 - 9.2
Chloride and Bromide as (Cl)	0.01% max.
Iodate IO ₃	To pass test (limit about 0.0003%).
Nitrogen Cpds. (as N)	0.001% max.
Phosphate (PO ₄)	0.001% max.
Barium (Ba)	0.002% max.
Calcium Magnesium & R ₂ O ₃ Precipitate	0.005% max.
Heavy Metals (as Pb)	0.0005% max.
Iron (Fe)	0.0003% max.
Sodium (Na)	0.005% max.
Seive Test # 20 U.S. Standard	25% max. through.

TABLE 11

DATA FROM KI/F₂ REACTIONS

Run	P _{F₂} (mm. Hg.)	10 ¹¹ C ₀ (ohm ⁻¹ cm. ⁻¹)	10 ⁹ C (ohm ⁻¹ cm. ⁻¹) after induc- tion period	10 ⁸ C _{max} (ohm ⁻¹ cm. ⁻¹)	t _{max} (hr.)	Appearance of pellet during reaction
L I	10	0.92	212.0 (at 20 hr.)	199.00	167	Dark brown earlier, be- came lighter with dark patches
L II	15	11.60	0.5 (at 7 hr.)	2.03	96	Light brown
L IV	30	0.95	---	35.00	55	At first light brown then decolourised
L V	30	2.35	0.87 (at 7 hr.)	0.33	73	"
L VI	30	4.10	0.65 (at 10.5 hr.)	411.00	256	"
L VII	30	0.24	---	22.90	30	Dark brown

TABLE 12
POLARIZATION BEHAVIOUR IN THE COURSE OF
KI/Cl₂ AND KI/F₂ REACTIONS

The values recorded for each run are polarization $f = \Delta E_2/E_2$, and the column headings are time in hours from the start of reaction.

Run	Reaction type	0	100	20/30	40/50	60/70	80/90	100/110	120
L II	A ₁								
L IV	A ₁	0.29		0.25	0.27				
L VI	A ₁								
S I	B	0.56	0.04	0.01			0.01	0	
S II	A ₁	0.54	0.63	0.49	0.66	0.58	0.56	0.53	
S III	A ₂	1.16		1.19	1.20				
S IV	A ₂	1.05	1.01	1.05					
S V	B, I ₂ added	1.63		0.88	1.57	1.25		1.49	1.70
S VI	B	0.66	1.19	1.26	0.76	0.51		0.36	0.29
S VII	B, I ₂ added	0.98		0.99	1.04				
L II	B, KI/F ₂	0.64		0.35	0.06	0.15			
L IV	B, KI/F ₂	1.15	0.56	1.19	0.12	0.05	0.18		
L VI	B, KI/F ₂	1.73	0.44		0.44		0.57	0.58	
L VII	B, KI/F ₂	1.66		0.14	0.13	0.23			
---	A ₁ , single crystal	0.33		0.36					

TABLE 13

INITIAL RISE IN CONDUCTANCE

Calculations for the first-order plot in Figure 18. The decay curve was first-order, $k_2 = 0.01478 \text{ hr.}^{-1}$. From extrapolation of decay curve to $t = 0$, $C'_\infty = 2.72 \times 10^{-9} \text{ ohm}^{-1} \text{ cm.}^{-1}$. From data tabulated below and plotted in Figure 18, $k_1 = 0.228 \text{ hr.}^{-1}$.

The calculation is self-consistent when the line is drawn through the points up to 5 hours as shown in Figure 18.

Check of self-consistency: from the initial slope of the reaction curve, $k_1 C'_\infty = 0.575 \times 10^{-9} \text{ ohm}^{-1} \text{ cm.}^{-1} \text{ hr.}^{-1}$. Hence,

$$C'_\infty = k_1 C'_\infty / (k_1 - k_2) = 2.70 \times 10^{-9} \text{ ohm}^{-1} \text{ cm.}^{-1}$$

t (hr.)	$k_2 t$	$e^{k_2 t}$	$10^9 C$	$10^9 C e^{k_2 t}$	$10^9 (C'_\infty - C')$	$\ln (C'_\infty - C')$
0	0	1	0	0	2.720	3.017
1	0.01478	1.015	0.586	0.596	2.120	2.772
2	0.0296	1.030	0.954	0.984	1.730	2.569
3	0.0443	1.045	1.245	1.301	1.410	2.362
4	0.0591	1.061	1.490	1.585	1.128	2.142
5	0.0739	1.076	1.710	1.840	0.874	1.883
6	0.0885	1.092	1.908	2.084	0.629	1.546
7	0.1033	1.109	2.054	2.280	0.436	1.188
8	0.1182	1.126	2.100	2.364	0.344	0.956

TABLE 14

TYPE B BEHAVIOUR IN AN I₂ ADDED KI PELLETT: $C \propto t^{2.5}$

Time after admission of Cl ₂ (min.)	$10^9 C$ ohm ⁻¹ cm. ⁻¹	$(10^{11} C - 2)^{0.4}$	Difference
0	0.02	0	
20	0.03	1	1:00
40	0.06	1.74	0:74
60	0.12	2.51	0:77
80	0.21	3.24	0:73
(100)	(0.32)	(3.90)	0:66
(120)	(0.49)	(4.65)	0:75
(140)	(0.70)	(5.40)	0:75
160	0.96	6.12	0:72
180	1.42	7.20	1:08

(Points indicated within brackets are uncertain, because they are read from a smoothed curve interpolated in a region with no experimental points.)

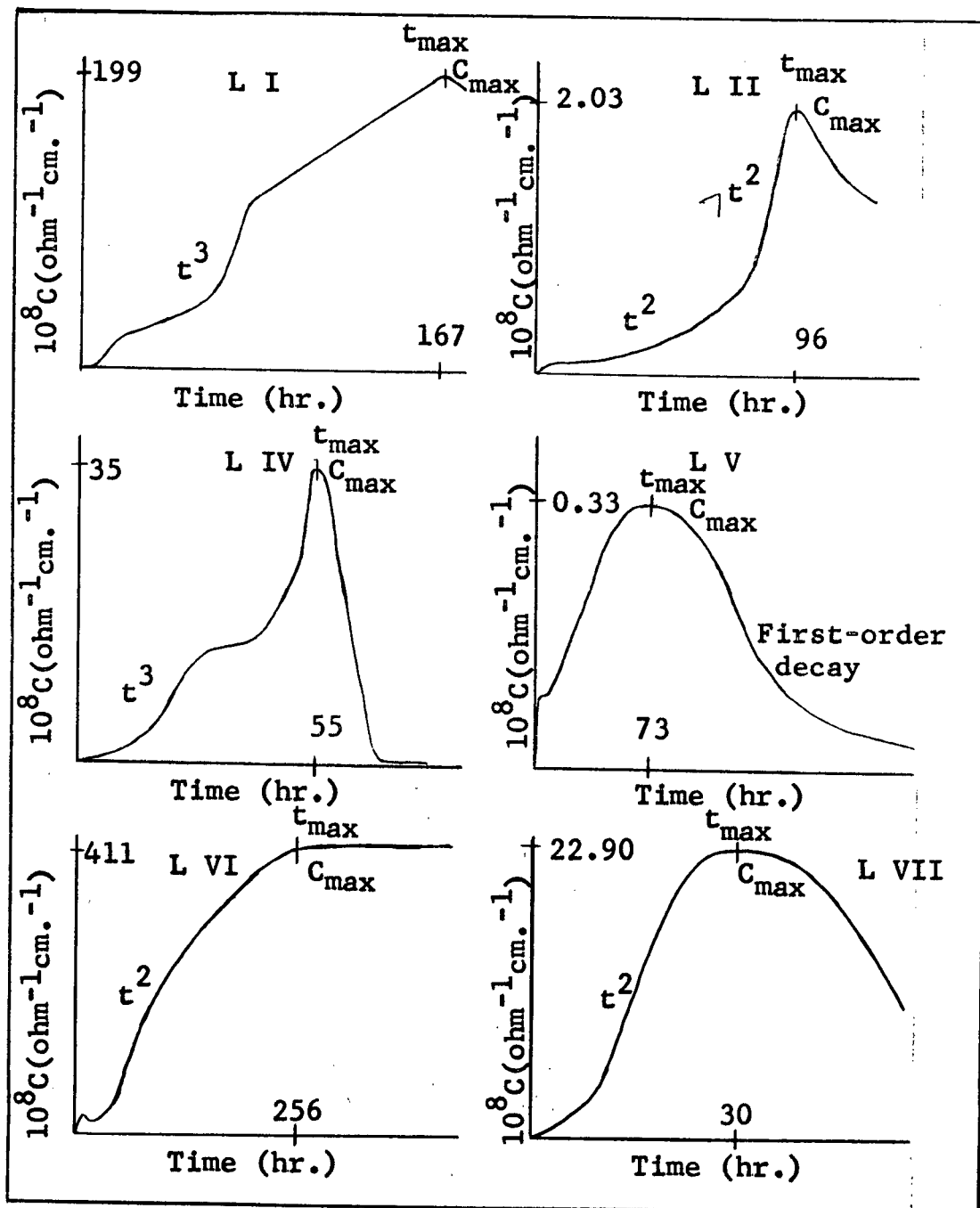
TABLE 15

HEIGHT OF FERMI LEVEL ABOVE CATION VACANCY LEVEL

AT THE END OF OXIDATION, FROM C_{∞}/C_0 .

Type of particle used in pellet	Type of behaviour	$10^{11}C_0$	$10^{11}C_{\infty}$	C_{∞}/C_0	$(E_f)_{\infty} - E_v$ (volts)
Large	A ₁	3.26	25.8	7.94	0.0031
Large	A ₁	6.24	20.2	3.24	0.0069
Large	A ₁	102	484	4.74	0.0049
Small	A ₁	83.1	218	2.62	0.0083
Small	A ₂	11,000	9,800	0.89	0.0193
Single Crystal	A ₁	1.85	0.519	0.28	0.0326
Small	B	0.13	94.5	715	--
Small, I ₂ added	B	8.94	1,520	170	--

FIGURE 26
SUMMARY OF KI/F₂ RUNS



BIBLIOGRAPHY

BIBLIOGRAPHY

1. Garner, "Chemistry of the Solid State". (Butterworth's Sci. Pubs., 1955).
2. Rees, "Chemistry of the Defect Solid State" (Methuen, London, 1954), p.93.
3. Wagner, Z. Phys. Chem., 1933, 321, 25.
4. Billington and Crawford, "Radiation Damage in Solids" (Princeton University Press, New Jersey, 1961), p.308.
5. Nowick, Phys. Rev., 1958, 111, 16.
6. Rabin and Klick, Bull. Am. Phys. Soc., 1959, 4, 147.
7. Morrison and Nakayama, Trans. Faraday Soc., 1963, 59, 2560.
8. Allnatt and Jacobs, Trans. Faraday Soc., 1962, 58 (Pt. I), No. 469.
9. Frenkel, ZS. f. Physik., 1926, 35, 652.
10. Brown and Seitz, Photographic Sensitivity, Vol. 2, ed. Fujisawa (Maruzen Co. Ltd., Tokyo, 1958), p.11.
11. Schulman and Compton, "Colour Centres in Solids" (Pergamon Press, 1963).
12. Wagner and Schottky, Z. Phys. Chem., 1930, 11(B), 163.
13. Schottky, Naturwissen, 1935, 23, 656.
14. Schottky, Z. Phys. Chem., 1935, 29(B), 335.
15. Jost, J. Chem. Phys., 1933, 1, 466.

16. Mott and Littleton, Trans. Faraday Soc., 1938, 34, 485.
17. Dreyfus and Nowick, J. of Applied Phys. Supplements,
1962, 33(1), 473.
18. Fumi and Tosi, Discussions Faraday Soc., 1957, 23, 92.
19. Pick and Weber, ZS. f. Physik., 1950, 128, 409.
20. Seitz, Revs. Mod. Physics., 1946, 18, 384.
21. Seitz, Revs. Mod. Physics., 1954, 26, 7.
22. Schokley, Hollomon, Maurier, and Seitz (editors), "Imperfections in Nearly Perfect Crystals" (John Wiley, New York, 1952).
23. Fumi (editor), "Supplements to Nuovo Cimento", Vol. VIII, Ser. x, No. 2 (Nicola Zanichelli, Bologna, 1958).
24. Mott (editor), Conf. on Defects in Crystalline Solids, The Physical Society, London, 1954.
25. Lidiard, J. Phys. Chem., 1958, 6, 298.
26. Dienes, J. Chem. Phys., 1948, 16, 620.
27. Tharmalingam and Lidiard, Phil. Mag., 1961, 6, 1157.
28. Dreyfus and Nowick, Phys. Rev., 1962, 126(4), 1367.
29. Lehovec, J. Chem. Phys., 1953, 21, 1123.
30. Eshelby, Newey, and Pratt, Phil. Mag., 1958, 3, 75.
31. Nagamiya, J. Phys. Soc., Japan, 1952, 7, 358.
32. Burstein and Oberly, Phys. Rev., 1950, 79, 903.
33. Varley, J. Nuclear Energy, 1954, 1, 130.

34. St. James, J. Phys. et Radium, 1956, 17, 907.
35. Harrison, J. Chem. Phys., 1963, 38(12), 3059.
36. Cohen, Phys. Rev., 1958, 107, 1096.
37. Känzig, Phys. Rev. Letters, 1960, 4, 117; J. Phys. Chem. Solids, 1960, 17, 80.
38. Luckey, Discussions Faraday Soc., 1959, 28, 113.
39. Luckey and West, J. Chem. Phys., 1956, 24, 879.
40. Mollwo, Ann. Phys., 1937, 29, 394.
41. Hersch, Phys. Rev., 1957, 105, 1410.
42. Hersch, J. Chem. Phys., 1957, 27, 1330.
43. Morrison and Nakayama, Trans. Faraday Soc., 1963, 59, 2560.
44. Catton, B.Sc. Thesis (unpublished), 1964.
45. Bird, B.Sc. Thesis (unpublished), 1963.
46. Uchida and Nakai, J. Phys. Soc. (Japan), 1954, 9, 928.
47. Nakai, J. Phys. Soc. (Japan), 1958, 13, 1424.
48. Harrison, Adams, Baijal and Bird, 5th, Int. Conf. on the Reactivity of Solids, Munich, 1964.
49. Adams, Ph.D. Thesis (unpublished), 1963.
50. Lehfeldt, Z. Phys., 1933, 85, 717.
51. Joffe, ZS. f. Phys., 1930, 62, 730.
52. Phipps and Partridge, J. Am. Chem. Soc., 1929, 51, 1331.
53. Cramer and Duncan, J. Chem. Soc., 1931, 2243.

54. McMorris and Yost, J. Am. Chem. Soc., 1932, 54, 2247.
55. Taft and Philipp, J. Phys. Chem. Solids, 1959, 3, 1.